

DIFFERENTIAL GALAXY EVOLUTION IN CLUSTER AND FIELD GALAXIES AT $Z \approx 0.3$ MICHAEL L. BALOGH¹, SIMON L. MORRIS^{2,5},
H. K. C. YEE^{3,5}, R.G. CARLBERG^{3,5}, AND ERICA ELLINGSON^{4,5}*ApJ, Accepted June 28, 1999*

ABSTRACT

We measure spectral indices for 1823 galaxies in the CNOC1 sample of fifteen X-ray luminous clusters at $0.18 < z < 0.55$, to investigate the mechanisms responsible for differential evolution between the galaxy cluster and field environments. The radial trends of D4000, $W_o(H\delta)$ and $W_o(OII)$ are all consistent with an age sequence, in the sense that the last episode of star formation occurred more recently in galaxies farthest from the cluster center. Throughout the cluster environment, galaxies show evidence for older stellar populations than field galaxies; they have weaker $W_o(OII)$ and $W_o(H\delta)$ lines, and stronger D4000 indices.

From our primary sample of 1413 galaxies, statistically corrected for incompleteness and selection effects, we identify a sample of K+A galaxies, which have strong $H\delta$ absorption lines ($W_o(H\delta) > 5 \text{ \AA}$) but no [O II] emission ($W_o(OII) < 5 \text{ \AA}$), perhaps indicative of recently terminated star formation. The observed fraction of $4.4 \pm 0.7\%$ in the cluster sample is an overestimate due to a systematic effect which results from the large uncertainties on individual spectral index measurements. Corrected for this bias, we estimate that K+A galaxies make up only $2.1 \pm 0.7\%$ of the cluster sample, and $0.1 \pm 0.7\%$ of the field. From the subsample of galaxies more luminous than $M_r = -18.8 + 5 \log h$, which is statistically representative of a complete sample to this limit, the corrected fraction of K+A galaxies is $1.5 \pm 0.8\%$ in the cluster, and $1.2 \pm 0.8\%$ in the field. Compared with the $z \approx 0.1$ fraction of 0.30% (Zabludoff et al. 1996), the fraction of K+A galaxies in the CNOC1 field sample is greater by perhaps a factor of four, but with only 1σ significance; no further evolution of this fraction is detectable over our redshift range.

We compare our data with the results of PEGASE and GISSEL96 spectrophotometric models and conclude, from the relative fractions of red and blue galaxies with no [OII] $\lambda 3727$ emission and strong $H\delta$ absorption, that up to $1.9 \pm 0.8\%$ of the cluster population may have had its star formation recently truncated without a starburst. However, this is still not significantly greater than the fraction of such galaxies in the field, $3.1 \pm 1.0\%$. Furthermore, we do not detect an excess of cluster galaxies that have unambiguously undergone a starburst within the last 1 Gyr. In fact, at $6.3 \pm 2.1\%$, the A+em galaxies that Poggianti et al. (1999) have recently suggested are dusty starbursts are twice as common in the field as in the cluster environment.

Our results imply that these cluster environments are not responsible for inducing starbursts; thus, the increase in cluster blue galaxy fraction with redshift may not be a strictly cluster-specific phenomenon. We suggest that the truncation of star formation in clusters may largely be a gradual process, perhaps due to the exhaustion of gas in the galactic disk over fairly long timescales; in this case differential evolution may result because field galaxies can refuel their disk with gas from an extended halo, thus regenerating star formation, while cluster galaxies may not have such a halo and so continue to evolve passively.

Subject headings: galaxies: clusters: general — galaxies: evolution — galaxies: stellar content

1. INTRODUCTION

The formation and evolution histories of the galaxies that populate rare, rich clusters are currently unknown; however, it seems unlikely that a single history can accurately describe the whole population (e.g., Hashimoto et

al. 1998). The giant elliptical galaxies which dominate the central regions of rich clusters seem to have been in place for well over 5 Gyr, and have only evolved passively since (e.g., Ellis et al. 1997, Bower, Kodama & Terlevich 1998, Barger et al. 1998). The remainder of the population is dominated in numbers by dwarf spheroidal galaxies and

¹Department of Physics & Astronomy, University of Victoria, Victoria, BC, V8X 4M6, Canada.
email: balogh@uvphys.phys.uvic.ca

²Dominion Astrophysical Observatory, National Research Council, 5071 West Saanich Road, Victoria, B.C., V8X 4M6 Canada.
email: Simon.Morris@hia.nrc.ca

³Department of Astronomy, University of Toronto, Toronto, Ontario, M5S 1A7 Canada.
email: hyee, carlberg@astro.utoronto.ca

⁴CASA, University of Colorado, Boulder, Colorado 80309-0389.
email: e.elling@casa.colorado.edu

⁵Visiting Astronomer, Canada-France-Hawaii Telescope, which is operated by the National Research Council of Canada, le Centre Nationale de la Recherche Scientifique, and the University of Hawaii.

in mass by early type galaxies (E, S0, early spirals). There is strong theoretical (e.g., Gott & Gunn 1972, Antonuccio-Delogu & Colafrancesco 1994, Van Haarlem & van de Weygaert 1993, Torman 1998) and observational (e.g., Zabludoff & Franx 1993, Henriksen & Jones 1996) evidence that much of the cluster galaxy population has been built up by the accretion of galaxies from the surrounding, low density, field environment, which implies that the rich cluster environment has affected a morphological change in these galaxies. A clear correlation between galaxy morphology with local density (Dressler 1980, Dressler et al. 1997) and cluster-centric radius (Whitmore, Gilmore & Jones 1993) has been observed. The well-known lack of emission line galaxies in clusters (Osterbrock 1960, Gisler 1978, Dressler, Thompson & Shectman 1985) has also been shown to correlate with cluster-centric radius (Balogh et al. 1997) and to be not entirely accounted for by the morphology–radius relation (Moss & Whittle 1993, Balogh et al. 1998). Recently, Abraham et al. (1996) and Morris et al. (1998) showed that these various effects could be interpreted as an “age” gradient, in the sense that galaxies farther from the cluster center formed part of their stellar component more recently than the central galaxies.

Another key piece of evidence that cluster galaxies are evolving strongly is the observation that the fraction of blue, spiral galaxies in clusters increases with redshift (e.g., Butcher & Oemler 1978, 1984, Dressler & Gunn 1983, Dressler et al. 1994, Couch et al. 1994, Rakos & Schombert 1995, Yee et al. 1995, Couch et al. 1998, but see Smail et al. 1998). This is usually referred to as the Butcher–Oemler (B–O) effect. To avoid possible misunderstanding, we will always refer to the B–O effect as this exclusively, a separate effect from the above problem of differential evolution between the cluster and field, though the two phenomena may be related. It has been shown that the star formation rate in the field also increases with redshift (Broadhurst, Ellis & Shanks 1988, Lilly et al. 1995, Rowan-Robinson et al. 1997, Tresse & Maddox 1998, Lin et al. 1999); thus, the B–O effect as we consider it here may not be an exclusively cluster-specific effect and cannot naïvely be used as an explanation of the different populations which inhabit cluster and field environments. Furthermore, it is not clear that the B–O effect can be directly interpreted as an evolutionary effect; Kauffmann (1995) has shown that rich clusters at $z \approx 0.4$ are not the direct progenitors of low redshift, comparably rich clusters. More recently, Andreon & Ettori (1999) have shown that the higher redshift Butcher–Oemler clusters have higher X-ray luminosities than their low redshift counterparts. Since fair samples of clusters generally show either no evolution, or even *negative* evolution in the X-ray luminosity function (e.g., Henry et al. 1992, Collins et al. 1997, Vikhlinin et al. 1998, Rosati et al. 1998), this confirms that the high redshift Butcher–Oemler clusters may not be the evolutionary predecessors of the low redshift clusters.

Various mechanisms may be responsible for the transformation of a star-forming field galaxy to a passively evolving cluster member. An infalling galaxy which passes through or near the center of the cluster may have much of its gas content stripped by the hot intra-cluster medium (ICM), following which star formation will cease (Nulsen

1982, Bothun & Dressler 1986, Balsara, Livio & O’Dea 1994). If only gas in an extended, diffuse halo is stripped, star formation may be allowed to continue by consuming the remaining disk gas but, without infall to replenish this supply, star formation will die out on timescales of a few Gyr (Larson, Tinsley & Caldwell 1980). Interaction with the ICM near the virial radius, where the ICM density is not high enough to completely strip the galaxy of its gas, may induce intense bursts of star formation (Dressler & Gunn 1983, Evrard 1991, Gavazzi & Jaffe 1987) which use up the remaining gas supply. Such bursts may also be induced by interactions with nearby galaxies (Moore et al. 1996, 1998, Fujita 1998) or, near the cluster center, by interactions with the tidal field of the cluster (Byrd & Valtonen 1990, Valluri 1993, Henriksen & Byrd 1996, Fujita 1998).

Understanding the mechanisms responsible for this change in star formation history is necessary to appropriately correct the CNOC1 universal mass density estimate (Carlberg et al. 1996) for the difference in mass-to-light (M/L) ratio in clusters, compared with the field. The correction applied in Carlberg, Yee & Ellingson (1997) could be compromised if a large number of cluster galaxies underwent strong starbursts which do *not* occur in the field population.

Dressler & Gunn (1983) identified a galaxy population which they later termed E+A galaxies, that have strong Balmer lines but no detectable emission lines. These galaxies (which we will hereafter term K+A to be consistent with current nomenclature) appear to have recently terminated star formation, within the ~ 1 Gyr prior to observation. As such, they play an important part in understanding the evolutionary history of galaxy populations. Evidence for these (and related) galaxies have been found both locally (Caldwell et al. 1993, Zabludoff et al. 1996) and at moderate redshift (e.g., Sharples et al. 1985, Lavery & Henry 1986, Couch & Sharples 1987, MacLaren, Ellis & Couch 1988, Broadhurst, Ellis & Shanks 1988, Fabricant et al. 1991, Abraham et al. 1996, Fisher et al. 1998, Morris et al. 1998, Dressler et al. 1999), in both cluster and field environments. Many authors have interpreted the presence of these galaxies as evidence that a large percentage of cluster galaxies recently underwent strong starbursts (e.g., Dressler & Gunn 1983, Couch & Sharples 1987, Barger et al. 1996, Poggianti & Barbaro 1996, Couch et al. 1998, Poggianti et al. 1999). However, it is still debatable whether or not starburst and post-starburst galaxies observed in clusters are unique to these environments. Furthermore, other authors have claimed that most K+A galaxies can largely be explained as the result of truncated star formation, without a large, initial burst (Newberry, Boroson & Kirshner 1990, Abraham et al. 1996, Morris et al. 1998). It is necessary both to distinguish between these two scenarios, and to compare their relative importance in the cluster and field environments, to determine which physical processes are plausible explanations for the differential evolution of cluster and field galaxies, and to determine how these processes will affect the M/L ratio in these environments.

The CNOC1 survey (Yee, Ellingson & Carlberg 1996) provides an excellent sample of galaxy spectra for which a reliable estimate of the star formation history for clusters

at $z \approx 0.3$ can be determined. This is a result of (1) a large sample size (over 2000 spectra); (2) well understood, and properly correctable, selection effects; (3) an identically selected field galaxy sample over the same redshift range; (4) objective measurements of spectral indices with well understood and empirically calibrated uncertainties; and (5) consistent comparison between data and spectrophotometric models. From these data, we will attempt to specifically address the following questions. First, what fraction of galaxies in the CNOC1 sample, regardless of environment, had significant star formation truncated in the last billion years or so? If this is truly larger than the low redshift fraction, it suggests a link with the B–O effect. Secondly, how does the abundance of these galaxies in the field compare with the abundance in clusters? An overabundance in clusters would suggest that the mechanism responsible for generating these galaxies may be what leads to the differential evolution of cluster and field galaxies. Finally, *how* is the star formation in these galaxies truncated? We will use spectrophotometric models to try to distinguish between a) truncation following a short burst; or, b) abrupt truncation without a burst.

The paper is organized as follows. In §2 we define our data sample and spectral index measurements. In particular, we discuss the details of our sample selection, statistical corrections, magnitude limits, and index uncertainties. Interpretation of our line indices is made based on a comparison with PEGASE (Fioc & Rocca–Volmerange 1997) spectrophotometric models, described in §2.4. Our galaxy classification scheme is presented in §3, and is based on the line indices of local galaxies and results of the PEGASE models (detailed in the Appendix). We present our results in various forms in §4, and take care to explore systematic effects which result from the large uncertainties on our line indices. In §5 we compare our results with the work of Zabludoff et al. (1996), Barger et al. (1996), Dressler et al. (1999) and others, and show that there is some consistency of results, though considerable variety in interpretation. We discuss some of the implications of these results in §6, and summarize our findings in §7.

2. OBSERVATIONS AND MEASUREMENTS

2.1. A Review of the Full CNOC1 Sample

The CNOC1 cluster sample consists of CFHT MOS images (Gunn g and r) and spectra of galaxies in the fields of fifteen⁶ X-ray luminous clusters in the redshift range $0.18 < z < 0.55$, selected from the EMSS survey⁷ (Gioia & Luppino 1994). The observational strategy and full details of the survey can be found in Yee et al. (1996). In particular, Yee et al. carefully consider and detail the selection effects of this sample, and describe how these are corrected for. For convenience, we repeat here some of the details in that paper relevant to the present analysis.

The spectra are obtained with the O300 grism in place, which results in a dispersion of 3.45\AA per pixel and cov-

ers the rest-frame wavelength range from (approximately) $[\text{OII}]\lambda 3727$ to the G-band ($\lambda \approx 4300\text{\AA}$) in most galaxies. Slits are $1''5$ wide, which results in a spectral resolution of about 16.5\AA FWHM. Images and spectra of galaxies in each cluster are obtained from either one, three or five MOS fields mosaiced east–west or north–south, which provide non-uniform coverage as far out as $1\text{--}2 R_{200}$ in projected distance for most clusters, where R_{200} is the radius ($\approx 1.2 \text{ h}^{-1} \text{ Mpc}$) at which the mean interior mass density is equal to 200 times the critical density, and within which it is expected that the galaxies are in virial equilibrium (Gott & Gunn 1972; Crone, Evrard & Richstone 1994). For $\Omega_0 = 0.2$, the cluster virial radius is equal to approximately $1.2R_{200}$. The final catalog contains redshifts for about 2500 galaxies, including field galaxies located in front of and behind each cluster.

In order to average over effects of non-sphericity, we will combine all fifteen clusters to produce a single sample, hereafter referred to as *the cluster*. Cluster membership is determined based on the observed radial velocity difference from the brightest cluster galaxy (BCG⁸). We use the mass model of Carlberg et al. (1997) to determine the (projected) radial dependence of the cluster velocity dispersion, $\sigma(r)$, from the average, measured dispersion, σ_1 . In Figure 1 we plot the galaxy velocities, normalized to σ_1 , against their projected radius from the BCG, normalized to R_{200} . The 3σ and 6σ contours of the mass model are shown as the solid and dashed lines, respectively. Galaxies with normalized velocities less than $3\sigma(r)$ are considered cluster members (squares), while those with normalized velocities greater than $6\sigma(r)$ comprise our field sample (circles). The population with intermediate velocities is represented by the solid triangles, and are considered “near-field”. The extent of the vertical axis in this figure is limited for clarity; hence only a small fraction of the total field population is displayed. The cluster population appears well separated from the field in this figure, and exhibits a rising velocity dispersion toward the cluster center. We will only include galaxies within $2R_{200}$ in our cluster sample, as larger radii are much more sparsely sampled.

By extracting the spectra with standard IRAF⁹ routines, an error vector is created which includes Poisson errors, read noise and sky subtraction uncertainties. This allows a good determination of both the signal-to-noise (S/N) ratio of the data, and also reliable errors on any measured quantities (see §2.2). The S/N ratio is defined as the mean value of the flux per pixel divided by the error per pixel, in the wavelength range $4050 < \lambda/\text{\AA} < 4250$. The resulting S/N distributions for the cluster and field samples are shown in Figure 2. The mode of the distribution is at $\text{S/N} \approx 7$ per pixel (or 15 per resolution element), and 94% of spectra have $\text{S/N} \gtrsim 3$.

The entire CNOC1 data sample, including the raw data and all measured quantities included in this paper, will

⁶Omitting cluster E0906+11, for which a velocity dispersion could not be computed due to an apparent double component structure(Carlberg et al. 1996).

⁷Except Abell 2390, which is not in the EMSS sample, but of comparable richness and X-ray luminosity to the other CNOC1 clusters (Abraham et al. 1996).

⁸Except for cluster MS 0451.5+0250, for which no redshift is available for the BCG. The velocities and positions are measured relative to the mean for this cluster.

⁹IRAF is distributed by the National Optical Astronomy Observatories which is operated by AURA Inc. under contract with NSF.

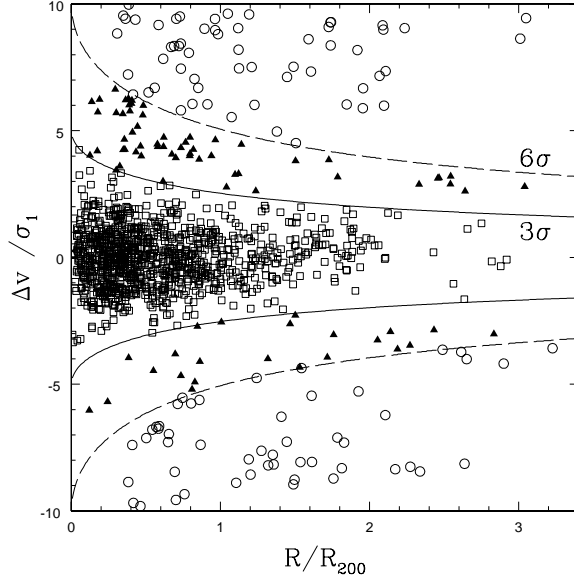


FIG. 1.— This figure shows how we define our cluster and field samples. The data plotted are radial velocity differences from the BCG, normalized to the cluster velocity dispersion, σ_1 , against projected radii from the BCG, in units of R_{200} . The *solid* and *dashed lines* are the $3\sigma(r)$ and $6\sigma(r)$ contours, respectively, of the cluster mass model of Carlberg et al. (1997). We define cluster members (*squares*) as those which lie within $3\sigma(r)$, and field galaxies (*circles*) as those with velocities greater than $6\sigma(r)$. The intermediate population (*solid triangles*) are termed “near-field”. The extent of the vertical axis is limited to clearly show the cluster population; only a small fraction of the field sample is shown in this figure.

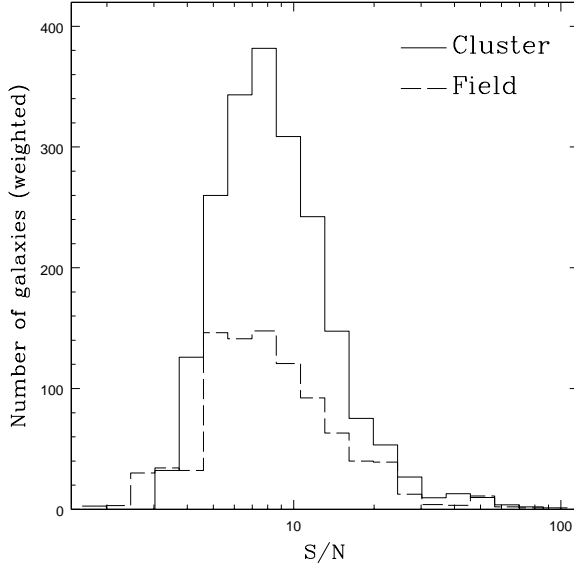


FIG. 2.— The distribution of signal-to-noise per pixel is shown for the cluster (*solid line*) and field (*dashed line*) samples. The number of galaxies in each bin is weighted as described in §2.3.1 and, thus, represents the number of galaxies in the photometric sample, though the distribution is computed from the spectroscopic sample.

soon be available from the Canadian Astronomy Data Centre (<http://cadcwww.hia.nrc.ca/>). All cosmologically dependent calculations in this paper are made assuming $q_0 = 0.1$, $\Lambda = 0$. The Hubble constant is parameterized as usual by $h = H_0/100 \text{ km s}^{-1} \text{ Mpc}^{-1}$.

2.2. Spectral Index Definitions

We will consider three spectral indices, tabulated in Table 1, which are automatically measured by an IRAF *IMFORT* routine available from the first author on request. The break strength at 4000Å (D4000) is defined as the ratio of the flux in the red continuum to that in the blue continuum. We have chosen a much narrower definition of this break than the standard definition (Hamilton 1985). There are two principal reasons for this. First, the uncertainty in the standard index value, assuming Poisson noise, was found to be a poor representation of the difference between multiple measurements of the same galaxy (this analysis is discussed further in §2.2.1). Reducing the width of the continuum definitions significantly improved this correspondence. Secondly, the new index is much less sensitive to reddening effects, which may be important (see §4.3.1).

There are considerable advantages in using D4000 instead of the available $g-r$ color. Most importantly, computing a rest frame color from the observed photometry requires calculating K-corrections from the very models we will be using to determine star formation histories and, thus, introduces a circular argument. Furthermore, the galaxy spectra are obtained from slits which only sample the central regions of the galaxy, while the photometry represents the integrated light from the whole galaxy. Thus, the photometric colors and observed spectral features may not arise from the same environments. (However, at $z = 0.3$, the slit width of 1.5'' corresponds to a linear size of $4.4h^{-1}$ kpc, which is a sizable region). In addition, especially for our unusually narrow definition of D4000, this index is very reddening insensitive. The principal disadvantage is that the measurement uncertainties in the D4000 measurements are generally larger than those of the $g-r$ colors.

The rest frame equivalent widths of the $H\delta$ Balmer absorption line, $W_o(H\delta)$, and the [OII] $\lambda 3727$ emission line, $W_o(OII)$, were automatically computed by summing the observed flux (accounting for partial pixels) above ($W_o(OII)$) or below ($W_o(H\delta)$) the continuum level, which itself is estimated by fitting a straight line to the flux in the continuum regions. The continuum data are weighted by the inverse square of the noise (from the IRAF noise vector), and the fit is then constructed by weighted linear regression. The blue and red continuum regions are defined in Table 1; the line flux is summed over the region defined “Line” in the same table. *Note that the $W_o(OII)$ index is positive when the line is in emission, while the $W_o(H\delta)$ index is positive when the line is in absorption.*

It must be noted that the indices defined above (or, indeed, any such indices) are not necessarily related simply or directly to physical quantities. The value of the $W_o(H\delta)$ index is very sensitive to the line and continuum definitions, and also on the spectral resolution and sampling. In particular, negative values of $W_o(H\delta)$ do not always indicate emission, since absorption lines in the continuum

regions (especially in galaxies with old stellar populations) may result in negative $W_o(H\delta)$ index values. Thus, caution must be taken when comparing these measurements with those of other authors; in fact, the index definition here differs slightly from that used by our own collaboration in Abraham et al. (1996).

2.2.1. Index Uncertainties

Errors on the spectral indices are determined from the noise vector generated from the optimal IRAF extraction. The D4000 index is simply a flux ratio and, hence, the error is determined from standard propagation techniques. Errors on equivalent width measurements are computed from equation A8 in Bohlin et al. (1983); this makes use of the uncertainties of the weighted, linear continuum fit, and the uncertainties of each pixel defined as comprising the line itself. Often, spectral regions contaminated by bright night sky line emission are very noisy, or interpolated over by hand. Since the computed error vector reaches very large values at the wavelengths of night sky lines, this effect will be reflected in the index uncertainties. Excluding from the sample all galaxies in which either of the lines at 5577 Å, 5890 Å, or 6300 Å lands within the index definitions of $H\delta$ or [O II] does not significantly change our main results.

Since spectra were obtained with up to three masks for each cluster and, also, since adjacent fields overlap by about 15'', some galaxies were deliberately observed more than once. This allows us to test the reliability of our error estimate, by comparing the difference between two measurements ($x_1 - x_2$) with the quadrature sum of their errors, $\sqrt{\sigma_1^2 + \sigma_2^2}$. In Figure 3 we plot the distribution of the ratio of these two numbers, $\epsilon = (x_1 - x_2)/\sqrt{\sigma_1^2 + \sigma_2^2}$, for each of the three indices. If the true errors are Gaussian distributed with a variance given by our error estimate, the distribution of ϵ should be Gaussian with a mean of zero and variance of unity; this is shown as the solid curve for reference. All of the ϵ distributions have a variance greater than 1, and are inconsistent with the solid curves. This implies that our raw uncertainties are underestimated, which may reflect the small but inevitable systematic error resulting from the subtraction of incorrect sky levels in some cases. The 3σ clipped variance of each ϵ distribution is 1.44 for $W_o(OII)$, 1.42 for $W_o(H\delta)$ and 1.96 for D4000. The distributions are better represented by a Gaussian of the corresponding, wider variance, shown as the dashed lines. To compensate for this effect, we multiplied all error estimates by the appropriate value. The final index value adopted for multiply observed galaxies is the average, weighted by the square of the error, of all independent measurements (up to three).

2.3. The Data Sample

In order to carry out our analysis, statistical weights must be computed for all galaxies, to correct for the incompleteness of the spectroscopic sampling; this procedure is reviewed in §2.3.1. We then proceed to define a luminosity-limited sample, in §2.3.2, which will be considered for those analyses which are sensitive to such a limit. For the remainder of the analysis, for which the primary purpose is to compare properties in the cluster and field

TABLE 1

Index	Blue continuum (Å)	Line (Å)	Red continuum (Å)
D4000	3850–3950	—	4000–4100
[OII] $\lambda 3727$	3653–3713	3713–3741	3741–3801
$H\delta$	4030–4082	4082–4122	4122–4170

NOTE.—Definitions of line indices measured on the data and spectrophotometric models. The D4000 index is the ratio of the flux in the red continuum to that in the blue continuum. The other three indices are equivalent widths of the line over the wavelength range listed in Column 3, where the continuum level is estimated from the flux blueward (Column 2) and redward (Column 4) of the line.

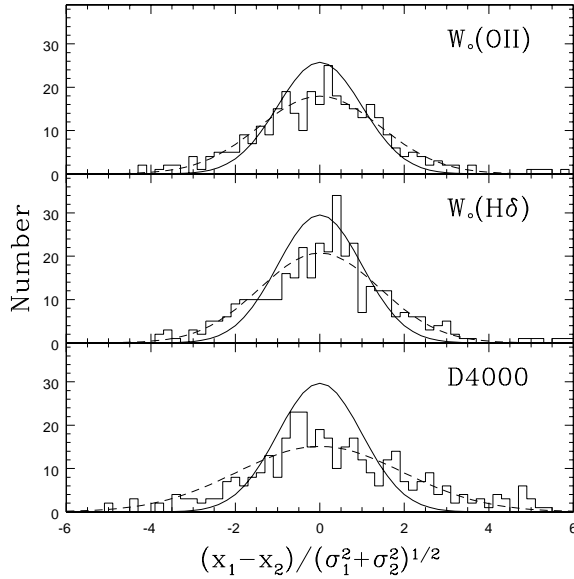


FIG. 3.— For multiply observed galaxies in the sample, we plot the ratio of the difference between two independent measurements of each index and the quadrature sum of the estimated index errors. If the true errors are normally distributed and well represented by the estimated errors, the distribution will be Gaussian with a mean of zero and variance of unity, shown by the *solid line*. The distributions are wider than this Gaussian, but consistent with one of variance 1.44 ($W_o(OII)$), 1.42 ($W_o(H\delta)$) and 1.96 (D4000), shown as the *dashed lines*.

samples, we define a larger sample which is not luminosity limited, but in which the lowest quality data are excluded, in §2.3.3. Unless otherwise specified, this latter is the data sample that will be discussed in the remainder of the paper.

2.3.1. Data Weights

Since spectra are not obtained for all of the galaxies observed photometrically, we must correct for this incompleteness and any selection effects that may arise as a result. These effects, and the calculation of compensating statistical weights, are considered in detail in Yee et al. (1996); we review them briefly here. The main selection criterion is apparent magnitude; a smaller fraction of faint galaxies are observed spectroscopically, relative to brighter galaxies. The magnitude weight W_m compensates for this effect. A second order, geometric weight W_{xy} is computed which compensates for such effects as the undersampling of denser regions, and vignetting near the corners of the chip. Finally, a color weight W_c is computed to account for the fact that bluer galaxies are more likely to show emission lines, facilitating redshift determination; however, this is a small effect, and we have checked that the inclusion of this weight does not significantly affect any of the results discussed in the present paper. Both W_{xy} and W_c are normalized so that their mean is 1.0 for the full sample. In all of our statistical analysis, each galaxy in our sample is weighted by $W_{\text{spec}} = W_m \times W_{xy} \times W_c$ to statistically correct for these selection effects¹⁰. We have also computed a “ring” weight, which is meant to correct for the fact that, due to the geometry of the cluster mosaics, the outer regions of clusters are less well sampled (in area) than the central regions. This correction is only important in the presence of radial gradients, if a globally averaged cluster quantity is sought. We will not use this weight in the present analysis, though we have verified that its use does not change any of the results (recall that we restrict the cluster sample to those galaxies within $R < 2R_{200}$).

2.3.2. Luminosity Limited Sample

We will first define a sample limited only in luminosity. Absolute r magnitudes (M_r) are calculated from the photometry, and k-corrections are made based on the $g-r$ colors and the model spectral energy distributions of Coleman, Wu & Weedman (1980), convolved with the filter response function, for four, non-evolving spectral types (E/S0, Sbc, Scd and Im). We also correct M_r for redshift evolution by assuming galaxies brighten by a factor (1+z) (Lilly et al. 1998; Abraham et al. 1998); thus, we correct all luminosities to the corresponding $z = 0$ values by dividing them by (1+z), though this does not significantly affect our results. We chose an absolute magnitude limit of $M_r = -18.8 + 5 \log h$, since this excludes most of the galaxies with large magnitude weights, $W_m > 5$; this limit corresponds to 1.8 mag below M^* in r (King & Ellis 1985). The absolute magnitude distribution of the cluster sample (weighted by W_{spec}) is compared with that of the field in Figure 4. There are 1125 galaxies in this sample (omitting the BCGs and cluster members beyond $2R_{200}$), including

710 cluster members, 343 field galaxies and 69 near field galaxies.

The absolute magnitude distributions of the low ($z \leq 0.33$) and high ($z > 0.33$) redshift galaxies in this sample are shown in Figure 5. As a result of the fainter apparent magnitude limit in the high redshift cluster samples (Yee et al. 1996), and the luminosity evolution correction, the two distributions are comparable.

2.3.3. The Maximal Sample

For the purposes of comparing cluster and field galaxy populations, it is desirable to use as much of the data as possible, excluding only that of the poorest quality, and ensuring that the luminosity distributions of the cluster and field samples remain similar. From the 1823 galaxies for which both [OII] $\lambda 3727$ and $H\delta$ lie within the observed redshift range (excluding the BCGs and cluster members beyond $2R_{200}$), we first select the 1572 which have $W_m \leq 5$, so that the lowest quality data do not dominate our results; this is equivalent to imposing a magnitude limit which varies from cluster to cluster. It is further desirable to remove those galaxies from the sample which have extraordinarily large uncertainties in the measured spectral indices, which often result from poor subtraction of bright night sky lines. The distribution of the error estimates for each index, scaled as discussed at the end of the previous subsection, are shown in Figure 6. Based on these distributions, we have chosen to exclude an additional 159 galaxies with errors greater than 15 \AA , 5 \AA , and 0.5 for $W_o(OII)$, $W_o(H\delta)$ and D4000, respectively. This selection introduces another second order correction to W_{spec} , as galaxies with index errors exceeding our limit tend to be fainter. We calculate, in bins of absolute luminosity, the fraction of galaxies, weighted by W_{spec} , removed from the sample by this selection. The remaining galaxies are weighted by the inverse of this number, which we will call W_{err} , multiplied by W_{spec} . W_{err} varies from 1 for galaxies with $M_r < -19.8 + 5 \log h$, to ~ 2 for galaxies with $M_r \approx -17.1 + 5 \log h$. The maximal sample consists of 1413 galaxies: 924 cluster, 407 field and 82 near field. The absolute magnitude distribution of the cluster sample (weighted by $W_{\text{spec}} \times W_{\text{err}}$) is compared with that of the field in Figure 7. Although the two distributions are similar, the cluster sample is biased toward less luminous galaxies, and the weights do not sufficiently correct the spectroscopic numbers (to be representative of the photometric sample) below $M_r = -18.8 + 5 \log h$, due to the removal of galaxies with $W_m > 5$.

2.4. The PEGASE Model Parameters

As discussed in § 2.2, the $W_o(H\delta)$ index is sensitive to its definition and the manner in which it is measured. Thus, its interpretation depends on comparing it with models in which the index is measured in an identical manner. It is not possible to use model results published by other authors (e.g., Couch & Sharples 1987, Barbaro & Poggianti 1997) to interpret data unless it is shown that the indices defined for those models are comparable to those defined

¹⁰All uncertainties in this paper that are based on \sqrt{N} Poisson statistics are computed from the unweighted number of galaxies under consideration.

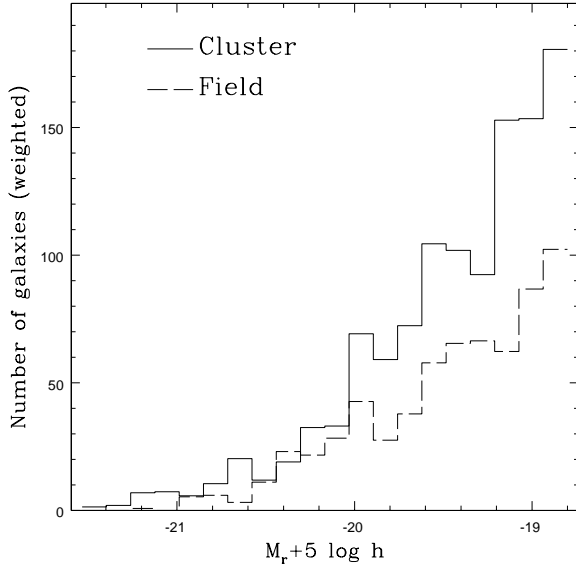


FIG. 4.— The evolution and k-corrected, absolute Gunn r magnitude distributions of the cluster (*solid line*) and field (*dashed line*), luminosity limited galaxy samples. Each bin is weighted by W_{spec} , discussed in §2.3.1; thus, the height of each bin represents the number of galaxies in the photometric sample, as determined from the spectroscopic sample.

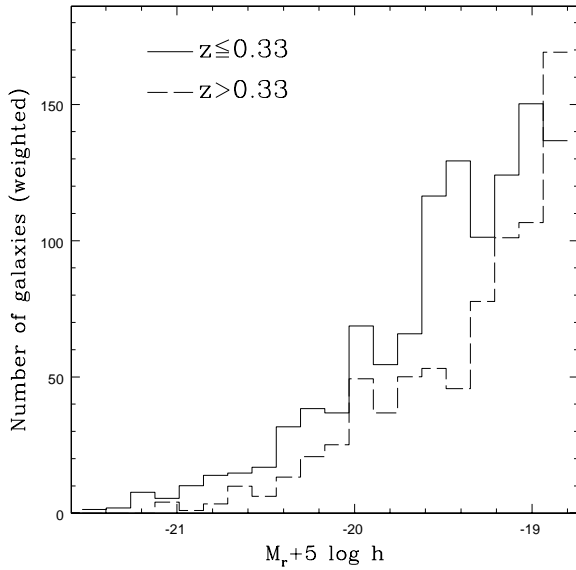


FIG. 5.— The evolution and k-corrected, absolute Gunn r magnitude distributions of the low redshift (*solid line*) and high redshift (*dashed line*), luminosity limited galaxy samples. Due both to the luminosity evolution correction, and to the fact that longer exposure times were used for the higher redshift clusters, the two distributions are similar. The histograms are weighted by W_{spec} ; see the caption of Figure 4.

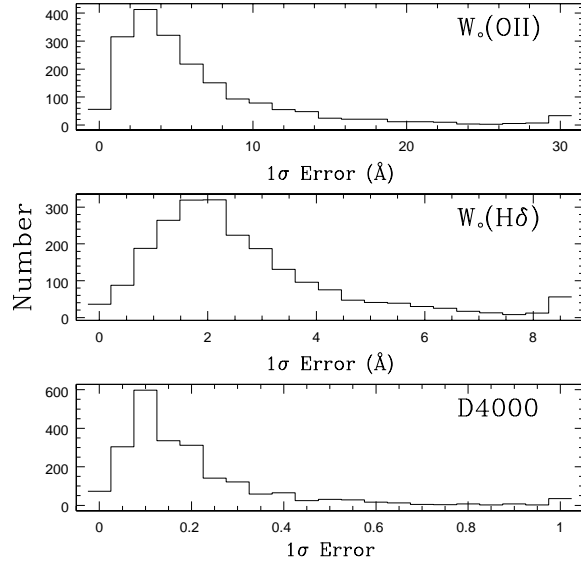


FIG. 6.— The distribution of 1σ errors on each of the three indices considered. In each case, the tail of the distribution extends to errors much greater than the mean. To avoid including data with very large uncertainties, we exclude the $\sim 10\%$ of galaxies with errors greater than 15\AA , 5\AA , and 0.5\AA for $W_o(OII)$, $W_o(H\delta)$ and D4000, respectively, in the maximal sample. This selection criteria is compensated for by a statistical weight, W_{err} , discussed in §2.3.3.

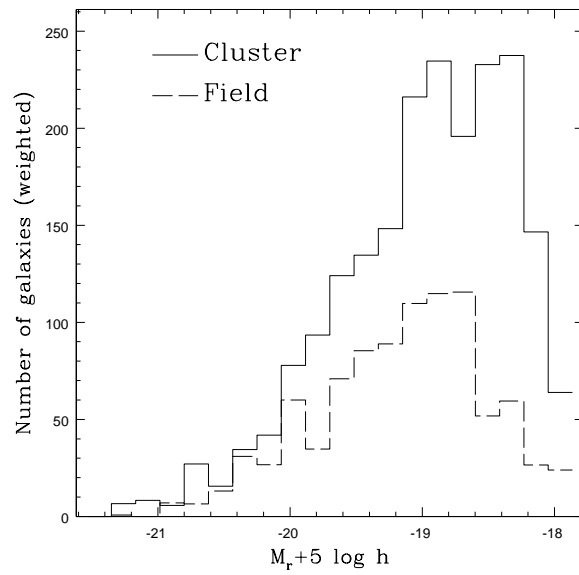


FIG. 7.— The evolution and k-corrected, absolute Gunn r magnitude distributions of the cluster (solid line) and field (dashed line) maximal galaxy samples (§2.3.3). The histograms are weighted by $W_{\text{spec}} \times W_{\text{err}}$, as discussed in the text. The cluster sample is biased to lower luminosities relative to the field sample, and a standard K-S test rejects the hypothesis that the two are drawn from the same population with $\sim 3\sigma$ confidence.

for the data. In light of this, we will reconstruct models in §3 which have been explored by other authors, but based on our index definitions.

The evolution of $W_o(H\delta)$ and D4000 with star formation history for solar metallicity galaxies is obtained from the PEGASE population synthesis code (Fioc & Rocca-Volmerange 1997), based on their UV to NIR spectral library. The PEGASE models predict results similar to those of the updated GISSEL96 models (Bruzual & Charlot 1993), but provide more freedom in constructing spectra with complex star formation histories; in particular, different initial mass functions (IMFs) are readily implemented. The drawback is that the models are solar metallicity; to investigate metallicity effects, we will consider the GISSEL96 models. The standard IMF adopted here is that of Salpeter (1955); the effect of adopting a truncated IMF model will be discussed in §4.3.1.

Spectral indices are determined from the model spectra in the same manner as from the CNOC1 data; that is, the same code, with the same line definitions, are run on the spectra output by PEGASE. We have not included Balmer-filling due to nebular emission; thus, the model $W_o(H\delta)$ indices represent an upper limit on the equivalent width one expects to observe when massive stars are present.

Care was taken to ensure that the line indices we obtain from the models correspond to the line indices measured on the data; in particular, the $W_o(H\delta)$ index is quite sensitive to both the resolution and the sampling of the spectra. The (rest frame) resolution of the model spectra is 10Å, comparable to the resolution of our data (about 15Å at $z=0.3$). However, the model spectra are more coarsely sampled than the CNOC1 data (every 10Å instead of every 2.6Å, rest frame), so we resample them to 2.6Å, interpolating using a fifth order polynomial fitting routine. We verified that each line index we measure on the CNOC1 spectra is unchanged if we first smooth the spectra by averaging every four pixels, and then resample using our interpolation algorithm.

3. GALAXY CLASSIFICATIONS

There is, as yet, no clear consensus in the literature about what type of galaxy is called, for example, a “starburst”, “H δ -strong”, “post-starburst”, “E+A/K+A”, etc. This is because the diagnostic indices are not all defined in the same way, the spectra used vary in terms of S/N and resolution, and the physical phenomena one is trying to isolate varies from author to author. In any case, such classifications are somewhat arbitrary, and there can be no objectively correct choice. For reasons discussed in §5, we have chosen not to use the most recent classification scheme (Dressler et al. 1999), and thus wish to state clearly how our classes are defined. These should be compared and contrasted not only with that paper, but also, for example, the differing definitions in Couch & Sharples (1987), Barbaro & Poggianti (1996), Barger et al. (1996) and Morris et al. (1998). In most cases, the differences in classification are ones of detail, and refined precision of the evolving nomenclature.

3.1. Determination of the $H\delta$ Threshold

One of the main goals of this paper is to identify a population of galaxies which were forming stars a short time (< 1 Gyr) ago, but have since stopped. These must be distinguished from galaxies which are currently undergoing star formation, and those which have not done so for a long time. We will make this distinction partly based on the spectra of local galaxies (see §3.2), and partly on model predictions, which is the purpose of this subsection.

In Figure 8 we show, as the dashed line, the evolution of the $W_o(H\delta)$ index for a galaxy with a constant star formation rate. As long as massive stars are present, nebular emission filling of H δ will reduce the index by between about 1Å and 3.5Å (Barbaro & Poggianti 1997); thus, such a spectrum will not reach $W_o(H\delta) \gtrsim 5$ Å. All normal, star-forming galaxies are therefore expected to have $W_o(H\delta) \lesssim 5$ Å, and nebular emission lines. This is confirmed by the line indices of normal, spiral galaxies, as we show in §3.2.

To reach $W_o(H\delta) > 5$ Å, the spectral light of a galaxy must be dominated by A- and early F-type stars. The presence of O- and B-type stars, which have weak intrinsic H δ absorption and can dominate the galactic light, is the reason why the dashed line in Figure 8 does not reach $W_o(H\delta) > 6.5$ Å, even without considering nebular emission contributions. For illustrative purposes, we show the evolution of $W_o(H\delta)$ in Figure 8 for a model galaxy with a constant star formation rate, but with no stars more massive than $2.7M_\odot$ (corresponding to an A0 star, Böhm-Vitense 1992). There will be no emission contribution to such a spectrum, which therefore has $W_o(H\delta) > 5$ Å for up to 7 Gyr; after that the accumulation of less massive stars, which have weak $W_o(H\delta)$ absorption, begins to contribute significantly to the light. Clearly the absence of OB-stars allows $W_o(H\delta)$ to reach much higher levels. As we will discuss in more detail in §3.3, strong $W_o(H\delta)$ indices may be observed following the abrupt termination of star formation, due to the almost immediate death of the O- and B-type stars. This can be visualized in Figure 8 as follows. A constantly star-forming galaxy will evolve at least ~ 1 Å below the dashed line; as soon as star-formation terminates, $W_o(H\delta)$ will increase approximately to the height of the solid line (which is an A-star dominated spectrum). For this reason, terminating star formation after 3 or 4 Gyr results in only a weak increase in $W_o(H\delta)$, while terminating a short burst of a few hundred Myr results in a much larger increase. In either case, emission lines will be absent in the spectrum.

Based on the results of these models, we adopt a threshold of $W_o(H\delta) = 5$ Å as an acceptable division between galaxies with normal rates of star formation, and those with recently truncated (or otherwise anomalous) star formation. This threshold is confirmed by the line indices of normal local galaxies, as discussed in the following subsection, and may be lowered to $W_o(H\delta) = 3$ Å for the reddest galaxies, as we demonstrate in §3.3.

3.2. Definitions Based on $W_o(OII)$ and $W_o(H\delta)$

We will classify the galaxies in our sample based principally on their position in the $W_o(OII)$ - $W_o(H\delta)$ plane relative to the PEGASE models, and to local galaxies. We show this plane in Figure 9. The data plotted are

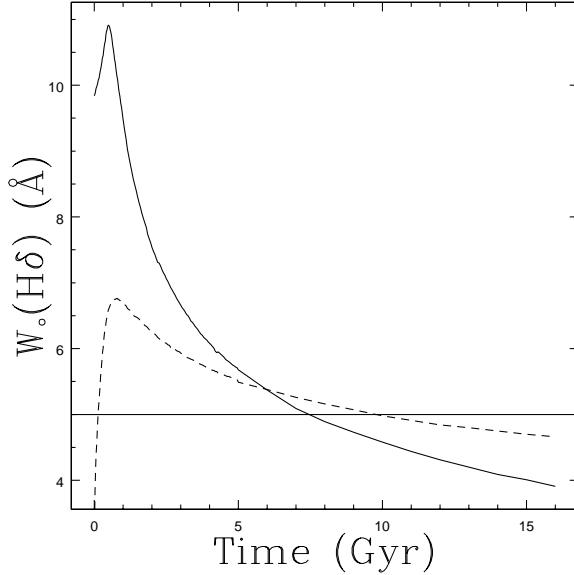


FIG. 8.— The evolution of $W_o(H\delta)$ with time, as determined from PEGASE models. The *dashed line* traces the evolution of a galaxy with a constant star formation rate, neglecting nebular emission, which will reduce $W_o(H\delta)$ by $\sim 1 - 3.5$ Å. The *solid line* is the same model, but without stars more massive than $2.7M_\odot$; there will be no emission contribution in this case. The horizontal line at $W_o(H\delta)=5$ Å is the lower $W_o(H\delta)$ limit for our K+A galaxy definition.

indices measured by running our code with our line definitions on the local data of Kennicutt (1992b, open symbols) and Kinney et al. (1996, filled symbols). The different symbols represent the different morphological classifications as shown on the figure. The diamonds include any galaxy classified as peculiar, irregular or starburst; all other points correspond to “normal”, local galaxies. The plane is divided into five regions, each of which we will discuss separately.

- **Passive Galaxy:** This is a galaxy that is not currently undergoing significant star formation, and thus evolves passively. Spectrally, we identify such a galaxy as one with $W_o(OII) < 5$ Å, which is roughly our detection limit, and $W_o(H\delta) < 5$ Å. The local galaxies in this category are mostly elliptical, S0 or early type spirals; the presence of these normal galaxies with $W_o(H\delta)$ as large as nearly 5 Å justifies the need for a threshold of at least this strength to clearly isolate galaxies with anomalous star formation histories.

- **Star Forming (SF) Galaxy:** This is a galaxy that has been undergoing significant star formation for at least several hundred million years. Unless heavily obscured by dust, the [OII]λ3727 emission line should be prominent, so $W_o(OII) > 5$ Å. Furthermore, models show that $0 < W_o(H\delta) < 5$ Å; the lower limit is determined from the results of Poggianti & Barbaro (1996) and Barbaro & Poggianti (1997), which show that, if star formation has been ongoing for at least several hundred million years, the stellar absorption will dominate any nebular emission of this feature. Local galaxies that lie in this

category are both late Spirals (Sc) and some galaxies that have been classified “starburst”, based on the presence of strong emission lines.

- **Short Starburst (SSB):** We define a short starburst as a *short lived* (< 200 Myr), *large increase* in star formation rate. A galaxy that has had a high star formation rate for more than a few hundred Myr will be considered a SF and *not* a SSB galaxy. In this case, nebular emission will dominate the $W_o(H\delta)$ feature and, hence, both $W_o(OII)$ and $W_o(H\delta)$ will be emission features (Poggianti & Barbaro 1996, Barbaro & Poggianti 1997).

- **K+A Galaxy:** This type of galaxy is one with no detectable [OII]λ3727 emission (defined as $W_o(OII) < 5$ Å), but strong Hδ absorption ($W_o(H\delta) > 5$ Å). Such a spectrum, which requires the presence of spectral type-A stars *without* more massive stars (which would give rise to [OII] emission lines), may be the result of a recently terminated episode of star formation, most likely following a short starburst (see, for example, Dressler & Gunn (1983), and §3.3). Alternatively, some of these galaxies may be extreme examples of the dust-obscured starburst scenario advocated by Poggianti et al. (1996) to describe the A+em galaxies (see below). This simple classification is based on only two line indices, and our K+A galaxies do not comprise a completely homogeneous class in terms of other spectral features, including the strength of other Balmer lines, or the Ca II H and K lines. This must be kept in mind when comparisons are made with other work in which these features are considered.

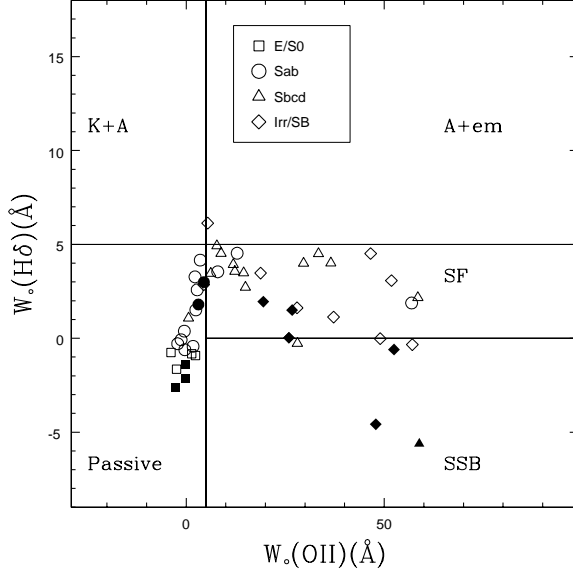


FIG. 9.— Local data of Kennicutt (1992b, *open symbols*) and Kinney et al. (1996, *filled symbols*) presented in the $W_o(OII)$ - $W_o(H\delta)$ plane. Positive values of $W_o(OII)$ and negative values of $W_o(H\delta)$ represent emission in these indices. The plane is divided into five regions according to the definitions in §3.2: Star-forming (SF) galaxies are those which have undergone significant star formation for at least several hundred Myr, while star formation in short starburst (SSB) galaxies has begun within about 200 Myr. The origin of A+em galaxies, which exhibit a strong A-star spectrum with emission lines, is uncertain; some may be dusty starbursts, or host an AGN. Of galaxies with $W_o(OII) < 5\text{\AA}$, K+A galaxies may have recently had their star formation truncated, while those galaxies with weaker $W_o(H\delta)$ indices are evolving passively, with little or no star formation.

- **A+em Galaxy:** Our final category consists of galaxies with $W_o(OII) > 5\text{\AA}$ and $W_o(H\delta) > 5\text{\AA}$. This corresponds to a galaxy with Balmer absorption lines as strong as those found only in A- and early F-type stars, but with [OII] $\lambda 3727$ emission lines indicating the presence of more massive O- and B-type stars. There is not yet a clear interpretation of these spectra; the presence of OB-stars should keep $W_o(H\delta) < 5\text{\AA}$ due both to emission-filling and the weaker, intrinsic $W_o(H\delta)$ absorption of these luminous stars. It is possible that some of the observed emission lines are due to an active nucleus; the useful diagnostic emission lines ($\text{H}\alpha, \text{H}\beta, [\text{N II}], [\text{O III}]\lambda 5007$) are generally redshifted out of our spectral range, so that we are unable to confirm this possibility. Alternatively, Poggianti et al. (1999) suggest that these galaxies (which they call e(a)) may be dust-obscured starbursts; we discuss this point further in §6, and note that the same interpretation may hold for the previously discussed K+A class of galaxy. The lone point in the Kennicutt (1992b) sample which lies in this region, shown on Figure 9, is NGC 3034, which is in fact a very dusty, star-forming galaxy. It has been classified “starburst” (e.g., Rieke et al. 1993) based on its strong $\text{H}\alpha$ emission, but has long been known to have an integrated stellar spectrum analogous to A-stars (e.g., Humason 1956); this galaxy would thus seem to be of the type advocated by Poggianti et al. (1999).

3.3. Additional Definitions Based on D4000

To investigate the physical origin of the K+A galaxies, we will compare our observations with the PEGASE spectrophotometric models to predict how $W_o(H\delta)$ evolves with galaxy color, as determined by the D4000 index. This largely follows the method outlined by Couch & Sharples (1987) and Barger et al. (1996), applied to the PEGASE models with our current index definitions.

Barger et al. (1996) divided their sample into red and blue halves at $B-R=2$ (observed at $z = 0.31$). To convert this to an equivalent cut in D4000, we calculate observed-frame ($z = 0.3$) $B-R$ and rest frame D4000 for two different star formation histories, using the PEGASE models. We show the results in Figure 10; the models are described in the caption. From this figure, we adopt D4000=1.45 as the value corresponding to $B-R=2$; this value is fairly independent (within 0.05) of the model considered.

We now plot the output of five different models in the D4000- $W_o(H\delta)$ plane, shown in Figure 11 and described briefly in the caption; we defer detailed discussion of these models to the Appendix. The local data plotted on this Figure are the same as those shown in Figure 9. The plane is divided into five regions similar to those defined by Barger et al. (1996), with the help of the D4000=1.45 division justified above. We have also renamed some of the classifications to correspond with our present terminology. The Passive, SF and SSB regions are expected to contain galaxies similar in star formation history to those

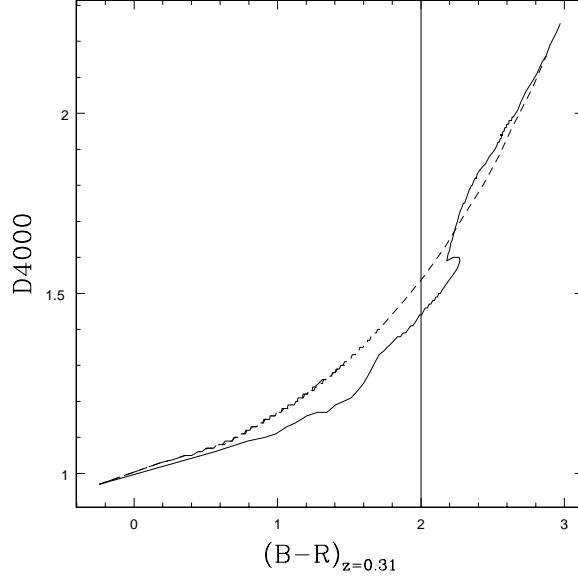


FIG. 10.— Observed frame $B-R$ is plotted against rest frame D4000 for two different PEGASE models. The *solid line* represents the evolution of a galaxy which formed all its stars in an initial, instantaneous burst. The *dashed line* corresponds to a galaxy with an exponentially decaying star formation rate, with an e-folding timescale $\tau = 2$ Gyr. The vertical line represents the division adopted by Barger et al. (1996), at $B-R=2$; we find this corresponds to $D4000 \approx 1.45$.

of the same name defined in §3.2. Galaxies with unusually strong $W_o(H\delta)$ indices are defined as either red or blue $H\delta$ -strong (rHDS or bHDS); these will include both K+A galaxies and A+em galaxies. Furthermore, normal galaxies in the red half of this plane generally show little or no sign of star formation; both the models and real data of galaxies redward of $D4000=1.45$ have $W_o(H\delta) < 3\text{\AA}$, and any contribution from nebular emission should be small. Therefore, we lower our $W_o(H\delta)$ threshold to 3\AA for the rHDS galaxies, as only the truncated star formation models pass through this part of the plane.

Both HDS categories will contain A+em galaxies, which have $W_o(OII) > 5\text{\AA}$. We discuss the suggestion by Poggianti et al. (1999), that these are dusty starbursts, in §6; whatever their origin, the A+em galaxies are not the result of truncated star formation, since such activity is still present. To isolate those spectra which most likely result from truncated star formation, we define two more galaxy classes, subsets of the rHDS and bHDS types:

- **Post-Starburst (PSB) Galaxies:** We define these to be bHDS galaxies with $W_o(OII) < 5\text{\AA}$. The PEGASE models shown in Figure 11 demonstrate that such a spectrum requires the termination of a short burst of star formation. Following this event, the galaxy spectrum will remain of the PSB type for about 300 Myr. Truncated star formation without a burst (the solid line) causes the spectrum to evolve quickly ($\lesssim 100$ Myr) through this region, and during much of this time emission lines will be present, reducing $W_o(H\delta)$ to values less than 5\AA . Thus, few (if any) bHDS galaxies are expected to result from truncated star formation without an initial starburst.

- **Post-Star Formation (PSF) Galaxies:** These are rHDS galaxies with $W_o(OII) < 5\text{\AA}$, and their spectra can be matched with either a recently terminated starburst episode, or through the abrupt cessation of longer term star formation. Galaxies evolving along either model track will spend about 300 Myr as a PSF galaxy; from the D4000 and $W_o(H\delta)$ indices alone, it is not possible to distinguish between these two possibilities.

3.4. Summary of Definitions

We have now defined six different types of “unusual” spectral types, based on models and the indices of local galaxies. All six of these types are rare, and can usually be matched by models in which star formation is truncated (T), sometimes following a short starburst (TSB); the galaxies with emission lines are not matched by either of these models, and are of uncertain origin (U). These six types, their definitions and interpretations are summarized in Table 2.

4. RESULTS

4.1. Spectral Index Dependence on Cluster-Centric Radius

The measured values of $W_o(H\delta)$, D4000 and $W_o(OII)$ in the maximal sample (§2.3.3) are shown in Figure 12, as a function of cluster-centric radius, R/R_{200} . Field galaxies are shown in the right hand panel of each graph, plotted against an arbitrary abscissa. The solid lines in each graph are the weighted median value for the field (right panel) and every 150 cluster points (left panel), with 2σ

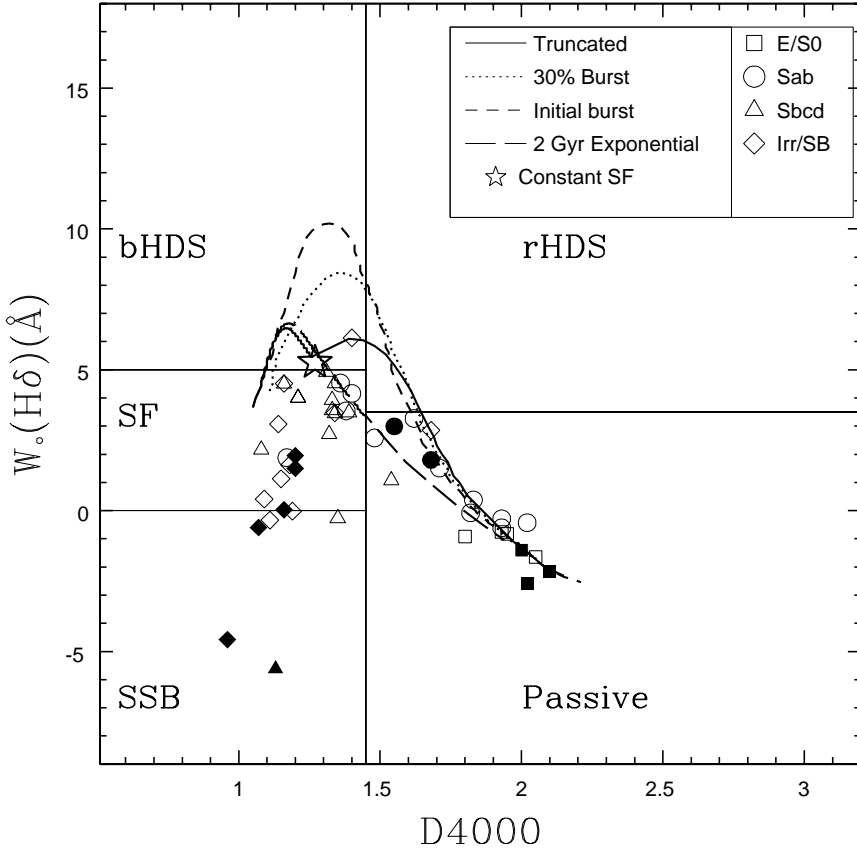


FIG. 11.— PEGASE models in the $D4000-W_o(H\delta)$ plane, for four different star formation histories which are discussed in the Appendix. Nebular emission contribution, not included in the models, will lower the $W_o(H\delta)$ index of any track with ongoing star formation, by at least 1\AA . A galaxy with a constant star formation is at the locus indicated by the *star*; an exponentially declining SFR gives rise to the evolutionary track traced by the *long-dashed line*. Truncating star formation in a galaxy with constant star formation at 4 Gyr causes it to evolve along the *solid line*. The *dashed line* shows an initial, instantaneous burst of star formation, while the *dotted line* represents a 200 Myr burst, involving 30% of the stellar population of a constantly star forming galaxy (all star formation is truncated following the burst). The plane is divided into SSB (short starburst), rHDS (red $H\delta$ -strong), blue HDS (blue $H\delta$ -strong), SF (star-forming), and Passive. The local data are from Kennicutt (1992b, *open symbols*) and Kinney et al. (1996, *filled symbols*).

TABLE 2

Type	$W_o(OII)$ (Å)	$W_o(H\delta)$ (Å)	D4000	Interpretation
K+A	< 5	> 5	—	T, TSB
A+em	> 5	> 5	—	U
bHDS	—	> 5	< 1.45	TSB, U
rHDS	—	> 3	> 1.45	T, TSB, U
PSB	< 5	> 5	< 1.45	TSB
PSF	< 5	> 3	> 1.45	TSB, T

NOTE.—Six spectral type classifications describing rare galaxy types which may be the result of recently terminated star formation. Column 5 lists compatible interpretations of each spectral type: *T*: Truncated star formation without an initial starburst; *TSB*: Truncated star formation following a burst; and *U*: Uncertain (due to the presence of emission lines).

jackknife errors (Efron 1981, Efron & Tibshirani 1986). In the central regions, all three indices are inconsistent with the corresponding field value with at least 2σ confidence, and they become increasingly field-like with increasing radius. The $W_o(H\delta)$ index shows a small increase from the center of the cluster out to R_{200} , significant at about the 2σ level; the decrease in D4000 over this range is measurable with about the same confidence. The median value of $W_o(OII)$ is roughly constant throughout the cluster, within 2σ limits, but clearly the total distribution changes more strongly; particularly striking is the near total absence of galaxies with $W_o(OII) > 20\text{Å}$ within $0.1 R_{200}$, as shown previously in Balogh et al. (1997, 1998). These trends are consistent with those observed in the individual clusters Abell 2390 (Abraham et al. 1996) and MS1621.5+2640 (Morris et al. 1998), and are qualitatively consistent with a model in which most cluster galaxies evolve passively, and the mean age of the galaxy stellar population decreases with increasing distance from the cluster center.

4.2. Galaxies in the $W_o(OII)$ – $W_o(H\delta)$ Plane

We plot $W_o(OII)$ and $W_o(H\delta)$ for the cluster and field (maximal) samples separately, in Figure 13. Each panel is divided into the same regions shown in Figure 9 and discussed in §3.2. The weighted percentage of galaxies in each region is shown, and the error associated with each number is determined assuming Poisson statistics. This error does not account for the uncertainty due to unequal scatter in this figure; we will address this issue in §4.2.1

The fraction of galaxies undergoing *some* type of star-formation (whether SF, SSB or A+em type) is $57 \pm 4\%$ in the field and only $29 \pm 2\%$ in the clusters. Despite the established B–O effect, the mean star formation rate in these clusters is less than that in the field, as discussed in Balogh et al. (1997; 1998). There is an apparent excess of K+A galaxies in the clusters compared with the field, significant at almost the 3σ level. As we will show in the next subsection, most or all of this difference can be attributed to the scatter in this figure, and to the slightly different absolute magnitude distributions of the cluster

and field samples. In particular, the systematic effects of scatter result in an overestimation of the K+A fraction; thus, we interpret the cluster fraction of $4.4 \pm 0.7\%$ as an upper limit. This is consistent with the results of other similarly defined samples at these redshifts, as we show in §5.

4.2.1. Determining the True K+A fraction

The large errors on both indices plotted in Figure 13 spread the data out in this plane; this results in non-uniform scatter since galaxies from the most populated regions (Passive and SF) will preferentially scatter into neighboring areas, biasing the fractions in these regions to larger values. In particular, the fraction of K+A galaxies, which occupy the high-end tail of the $W_o(H\delta)$ distribution, will be overestimated, and we can expect this effect to be larger in the cluster sample, where the Passive galaxy population is more dominant than in the field. We can demonstrate this by assuming that the true distribution of Passive galaxies is the same in both the cluster and the field though the absolute number of such galaxies in each environment is different. Thus, the $W_o(H\delta)$ distribution of galaxies with $W_o(OII) < 5\text{Å}$ should be the same if the fraction of K+A galaxies is also identical. In Figure 14, we show these distributions normalized to unit area in the top (field) and middle (cluster) panels. Subtracting the cluster bins from the field bins yields the distribution shown in the lower panel. This allows easy comparison of the shapes of the $W_o(H\delta)$ distribution in the cluster and field samples: a relative excess of cluster galaxies with a given $W_o(H\delta)$ would result in a negative value in the bottom panel of this figure. Instead, we see that the fraction of galaxies with $W_o(H\delta) > 5\text{Å}$, corresponding to the K+A galaxies, is not significantly different in the two samples. That is, the difference between the (normalized) cluster and field samples in the two bins with $W_o(H\delta) > 5\text{ Å}$ is equal to zero within the 1σ errors. There is a 1σ excess of field galaxies with $W_o(H\delta) \approx 3\text{ Å}$, which suggests that even “passive” galaxies in the field may have somewhat younger stellar populations than similar galaxies in clusters.

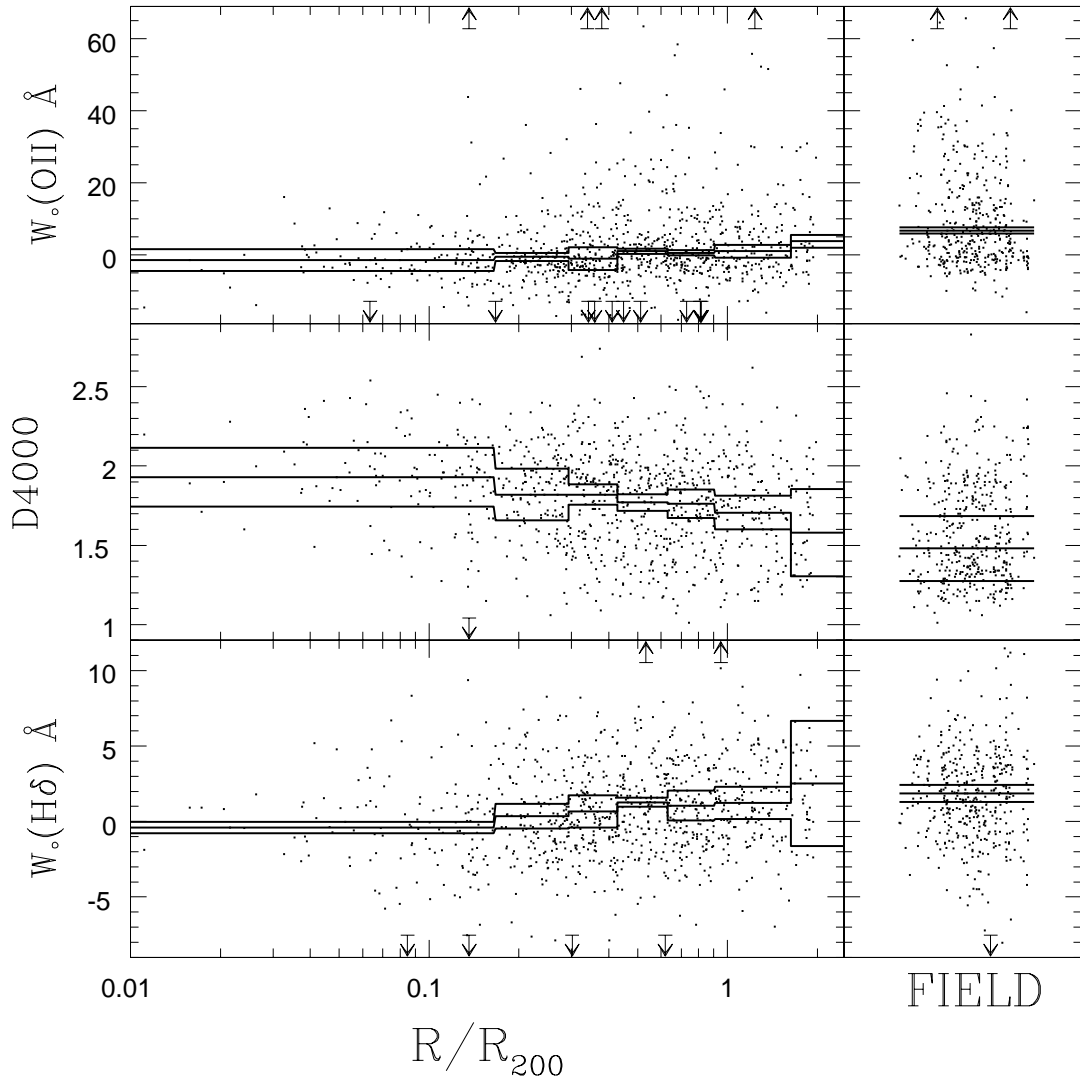


FIG. 12.— Spectral indices plotted as a function of cluster–centric radius. The sample displayed in the right hand panels is the field galaxy sample, plotted against an arbitrary abscissa for display purposes. Positive values of $W_o(OII)$ and negative values of $W_o(H\delta)$ represent emission in these indices. The *solid lines* are the median index value for every 150 cluster galaxies, and the 2σ jackknife error estimates. The range of data shown is restricted to clarify the characteristics of the bulk of the data; arrows indicate data which lie outside the plotted regions.

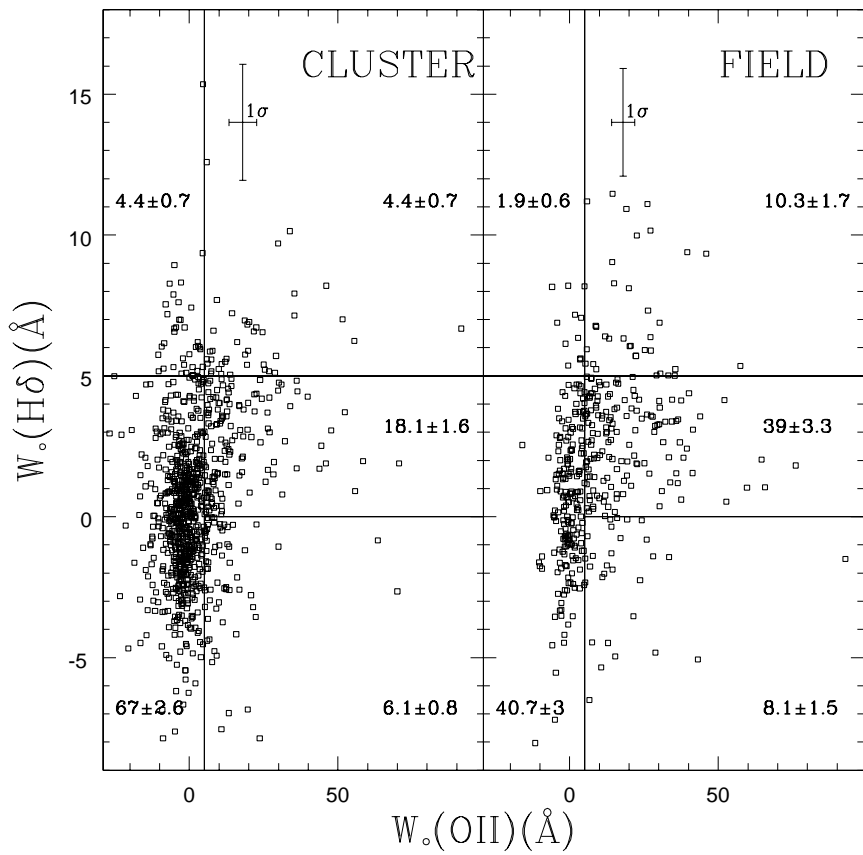


FIG. 13.— The cluster and field data presented separately in the $W_o(OII)$ - $W_o(H\delta)$ plane, which is divided into regions defined in Figure 9 and discussed in §3.2. Positive values of $W_o(OII)$ and negative values of $W_o(H\delta)$ represent emission in these indices. The sample error bars represent the mean 1σ error, and the number in each region represents the weighted percentage of galaxies in that region. The errors assume Poisson statistics, and do not account for the nonuniform scatter of data points throughout the plane; see §4.2.1 for details of this effect.

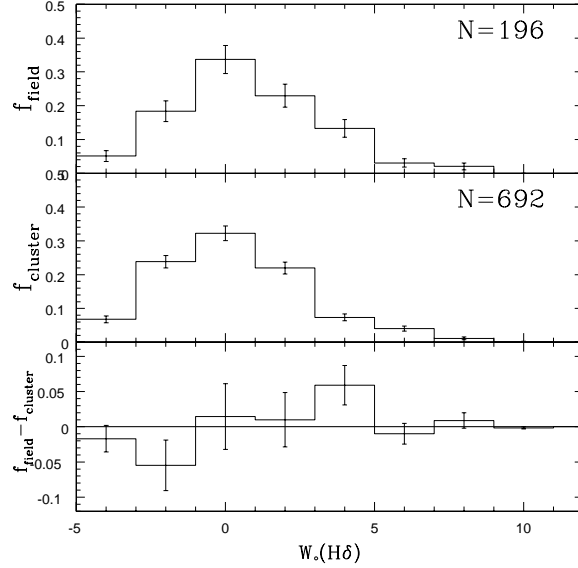


FIG. 14.— The distributions of $W_o(H\delta)$ for the subsample of galaxies with $W_o(OII) < 5\text{\AA}$ are shown for the field (*top panel*) and cluster (*middle panel*), normalized to unit area. The number of galaxies in each sample is shown in the top right corner; all error bars are 1σ , assuming Poisson statistics. The difference between these two distributions is shown in the *bottom panel*. There is no excess of cluster galaxies with $W_o(H\delta) > 5\text{\AA}$, which correspond to the K+A galaxies, relative to the field.

We will now estimate a correction for the fractions in each of the regions of Figure 13. The only way that a precise correction can be made is if the *a prior* distribution is known, which is not the case here; therefore, some assumptions about this distribution will have to be made. We will consider two different methods of obtaining this correction: the first is applicable to each galaxy class, but requires stronger assumptions, while the second method provides a more robust estimate but is only valid for the K+A galaxies.

Method 1: Monte Carlo Simulations: We could estimate the effects of scatter by adding appropriate noise to a “pure” sample with no scatter. We attempt to approximate such a sample by selecting galaxies with reasonably high signal-to-noise measurements ($S/N > 5$) and errors in both indices which are below the 25th percentile ($\Delta W_o(OII) < 2.5\text{\AA}$ and $\Delta W_o(H\delta) < 1.5\text{\AA}$). Admittedly, this is not quite what we want, as it is quite possible that this subsample (generally with higher luminosities) is not distributed like the full sample; however, it should give an approximately accurate correction, as confirmed by the second method described below. These data are shown in the bottom panel of Figures 15 and 16 for the cluster and field samples, respectively.

We now simulate noisy cluster and field samples by adding Gaussian random noise, with a variance chosen randomly from the 1σ uncertainties of the full (cluster or field, as appropriate) data sample. We then generate several realizations, each one containing a number of points equal to the number in the true cluster or field sample. One such simulation is shown in the top panels of Figures 15 and 16. From twenty realizations, we determine, for each

galaxy class, the average difference between the fraction of such galaxies in the noisy (simulated) and true (low-error sample) distributions, and the variance of that difference. We will refer to this value as the “scatter correction”.

In Table 3, we show the measured fraction of each galaxy type, from Figure 13, in columns 2 (cluster) and 5 (field). Columns 3 and 6 show the estimated scatter correction. Subtracting these numbers from the appropriate measured value, including the error in this correction, yields the corrected fractions in columns 4 and 7.

We note that, in Table 3, the corrected K+A fraction is equal to zero within 2σ uncertainties. However, this does *not* mean that K+A galaxies are not present in the sample; to provide concrete examples we show, in Figure 17, sample spectra for two K+A galaxies: one found in the field and one in the cluster. Note that the Ca II K line, prominent in the bottom spectrum, is weak/absent in the top spectrum; this is an example of two galaxies which are assigned the same classification (K+A), though their spectra are not identical.

Method 2: Gaussian Cloud Analysis: An alternative way to determine the overestimate of the K+A fraction is to assume that it is due only to scatter in the $W_o(H\delta)$ direction from the Passive galaxies, i.e. those with $W_o(H\delta) < 5\text{\AA}$ and $W_o(OII) < 5\text{\AA}$. We can represent the $W_o(H\delta)$ index of each galaxy as a Gaussian probability function, with variance given by the 1σ index uncertainty. For each galaxy in the Passive sample, we calculate the probability that $W_o(H\delta) > 5\text{\AA}$, and then compute the weighted sum of all these probabilities. A smaller amount of “backscatter” (from the K+A region to the Passive) will also take place, and this must be subtracted off in an

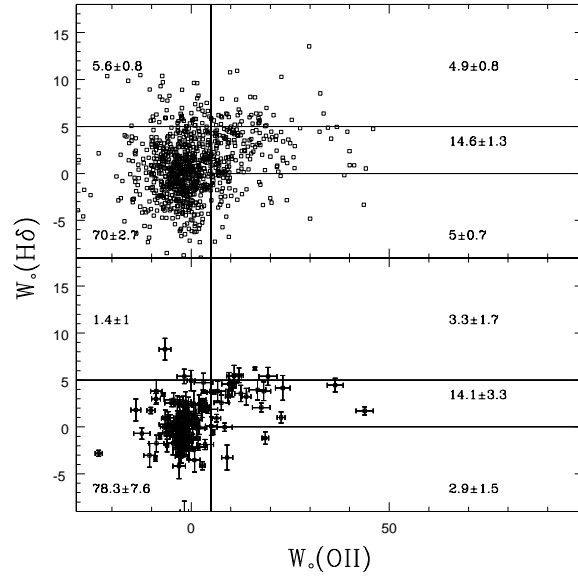


FIG. 15.— The *bottom panel* shows cluster data with $S/N > 5$, and errors in $W_o(H\delta)$ and $W_o(OII)$ less than 1.5\AA and 2.5\AA , respectively. Error bars are 1σ . We add noise, characteristic of the full sample error distribution, to each point, and generate twenty realizations containing the same number of data points as the full cluster sample. One such realization is shown in the *top panel*. The plane is divided into the same regions defined in Figure 9; the numbers in each panel are the weighted percentage of objects in that bin. This experiment is used to calculate the scatter correction given in Table 3.

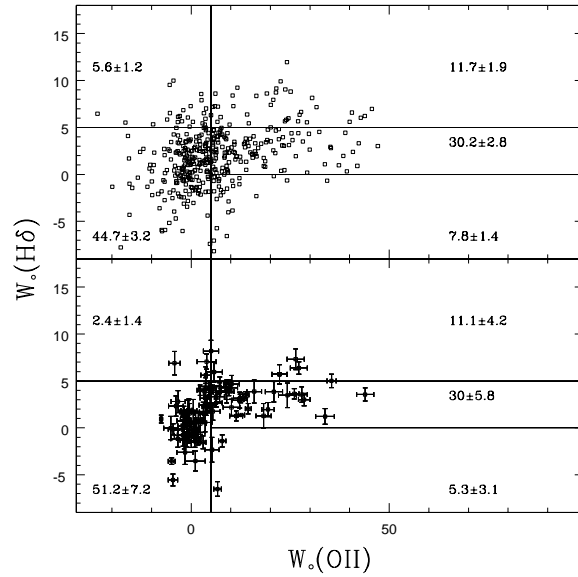


FIG. 16.— This is the same as Figure 15, but for the field sample. Again, the results are tabulated in Table 3.

TABLE 3
SYSTEMATIC ERROR ESTIMATIONS IN THE $W_o(OII)-W_o(H\delta)$ PLANE

Object Type	Cluster (%)			Field (%)		
	Measured	Scatter	Corrected	Measured	Scatter	Corrected
K+A	4.4 ± 0.7	2.8 ± 0.5	1.6 ± 0.9	1.9 ± 0.6	2.2 ± 0.9	-0.3 ± 1.1
A+em	4.4 ± 0.7	1.4 ± 0.5	3.0 ± 0.9	10.3 ± 1.7	4.0 ± 1.3	6.3 ± 2.1
SF	18.1 ± 1.6	-2.4 ± 0.6	20.5 ± 1.7	39.0 ± 3.3	-3.3 ± 2.2	42.3 ± 4.0
Passive	67.0 ± 2.6	-7.1 ± 1.0	74.1 ± 2.8	40.7 ± 3.0	-6.2 ± 1.4	46.9 ± 3.3
SSB	6.1 ± 0.8	5.0 ± 0.8	1.1 ± 1.1	8.1 ± 1.5	3.4 ± 1.4	4.7 ± 2.1

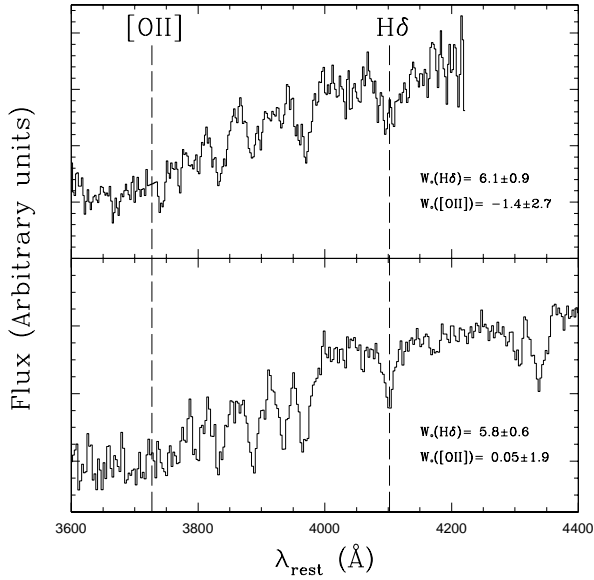


FIG. 17.— Two high S/N examples of galaxies in our sample with a K+A type spectrum, in the rest frame. The *bottom panel* shows a cluster member in Abell 2390 at $z = 0.2211$ (S/N=22, ppp #100537); the *top panel* shows a field galaxy in the field of MS1512 at $z = 0.4926$ (S/N=7, ppp #200607). These are good quality spectra, and not characteristic of typical spectra in the CNOC1 sample. Note that, although both galaxies are classified as K+A, the top spectrum lacks the strong Ca II K line present in the bottom spectrum.

analogous manner. This difference would give the total fraction of galaxies which have scattered from the Passive region into the K+A region, if the distribution of data in this plane was representative of the error-free distribution; since the uncertainties significantly blur this distribution, this difference results instead in the *maximum* amount of K+A “contamination” expected. Following this procedure, we determine that the maximum correction to the K+A fraction should be 2.8% for the cluster, and 2.5% for the field (appropriate for the maximal data sample of §2.3.3).

We can now estimate the *minimum* correction required by counting the weighted number of Passive galaxies with $W_o(H\delta) < -5\text{ \AA}$. Since the mean $W_o(H\delta)$ in the Passive region is greater than zero, and we expect few if any Passive galaxies to actually have $W_o(H\delta) < -5$, this fraction of galaxies represents the minimum amount of scatter into the K+A region (without a backscatter correction). For the maximal cluster sample, this minimum correction is 1.9%; for the field, it is 1.2%.

If we adopt the average of the minimum and maximum corrections, and half the difference to represent (arbitrarily) a 2σ uncertainty, we determine the best correction to be $2.3 \pm 0.25\%$ for the cluster, and $1.8 \pm 0.3\%$ for the field, resulting in corrected K+A fractions of $2.1 \pm 0.7\%$ and $0.1 \pm 0.7\%$, respectively. These corrections are somewhat smaller than the ones in Table 3, but equivalent within the uncertainties. Although we take this method to be the more robust estimate for the K+A correction, it confirms that the corrections listed in Table 3 are likely to be reasonable estimates.

Luminosity Limit: In Figure 18 we show the M_r distribution of the K+A sample, compared with the overall distribution of the maximal sample. This figure shows that many of the K+A galaxies lie below $M_r = -18.8 + 5 \log h$, where the magnitude weights are large, and the maximal sample is not statistically representative of a complete photometric sample. Thus, any absolute evaluation of the K+A fraction will be sensitive to the magnitude limit and statistical correction. In consideration of this, we show the results for the luminosity limited sample (§2.3.2) in Figure 19. For this restricted sample, the fraction of K+A galaxies is equal to $3.3 \pm 0.7\%$ in the cluster, and $2.7 \pm 0.8\%$ in the field; the two are equivalent within 1σ uncertainties. Adopting the Gaussian cloud scatter correction (Method 2), we find that these two numbers are overestimated by $1.8 \pm 0.4\%$ and $1.5 \pm 0.3\%$, respectively; thus, the true fraction is reduced to $1.5 \pm 0.8\%$ in the cluster, and $1.2 \pm 0.8\%$ in the field.

Summary of Corrected Values: Although the amount of scatter correction necessary cannot be precisely determined (since the true distribution of the data is unknown), the uncorrected, cluster K+A fraction of $4.4 \pm 0.7\%$ is a secure upper limit. Our best estimate of the true K+A fraction is thus obtained by applying the corrections determined by the Gaussian cloud estimate. For the maximal galaxy sample, we find the fraction of K+A galaxies is $2.1 \pm 0.7\%$ in the cluster, and $0.1 \pm 0.7\%$ in the field. For the luminosity limited sample, the fraction is $1.5 \pm 0.8\%$ (cluster) and $1.2 \pm 0.8\%$ (field). We conclude that, once scatter and luminosity effects are accounted for, there is no significant difference between the frequency of

K+A galaxies in the cluster and field environments. We will compare these numbers with the results of other surveys, both locally and at similar redshifts, in §5.

4.2.2. The Radial Dependence

The fraction of each galaxy type is plotted as a function of distance from the center of the cluster, normalized to R_{200} , in Figure 20. The three “active” classes SF, A+em and SSB have been grouped together for clarity. We have corrected each value for the estimated effects of scatter, using Method 1 in §4.2.1, and included the uncertainty of this correction in the error bars. The galaxy population within the cluster exhibits a steadily increasing fraction of passively evolving galaxies and a steadily decreasing fraction of star forming galaxies with decreasing radius. This is at least partly expected from the morphology–density relation (Dressler 1980) but, as shown in Balogh et al. (1998) this relation cannot completely account for the decrease in star formation rate toward the center of the cluster. The fraction of K+A galaxies within the cluster is never significantly in excess of the field value, at any radius.

4.2.3. The Redshift Dependence

The fifteen clusters in the CNOC1 sample cover a large range in redshift, from 0.18 to 0.55 and, thus, it is of interest to investigate the possible redshift dependence of the populations. To ensure an equitable comparison, we consider the luminosity limited sample (§2.3.2) here (recall that an evolution correction is applied to the luminosities). First, we show in Figure 21 the redshift distribution of this sample, separately for the cluster and field. This figure shows that the cluster observations are well divided into three, well populated redshift bins: $0.15 < z < 0.28$; $0.28 < z < 0.35$; and $0.35 < z < 0.7$.

In Figure 22 we plot the fraction of each galaxy type, as defined in §3.2 and Figure 13, in each of the three redshift bins described above. Again, we have grouped all star-forming galaxies together (SF, A+em and SSB) for clarity, and corrected the values for the systematic effects of scatter using Method 1 of §4.2.1. The cluster sample is shown in the bottom panel, and the field in the top panel. A small increase in the fraction of star forming galaxies with redshift is observed, though only significant at about the 1σ level. Importantly, the abundance of K+A galaxies does not show an increase with redshift, which shows that the smallness of the fraction we observe is not just due to the fact that our sample is dominated by low redshift $z \approx 0.2$ galaxies.

4.2.4. The Near-Field Galaxies

In Figure 23 we show the $W_o(OII)$ - $W_o(H\delta)$ relation for the near-field galaxies in the luminosity limited sample (§2.3.2). The near-field galaxies are a subset of galaxies with velocities intermediate between our cluster and field definitions (between 3 and 6 times the cluster velocity dispersion), and will include both galaxies that are far from the cluster (≈ 50 Mpc), with velocity differences that reflect the Hubble flow, and infalling galaxies with peculiar velocities in excess of three times the cluster velocity dispersion. None of the galaxy abundances are significantly

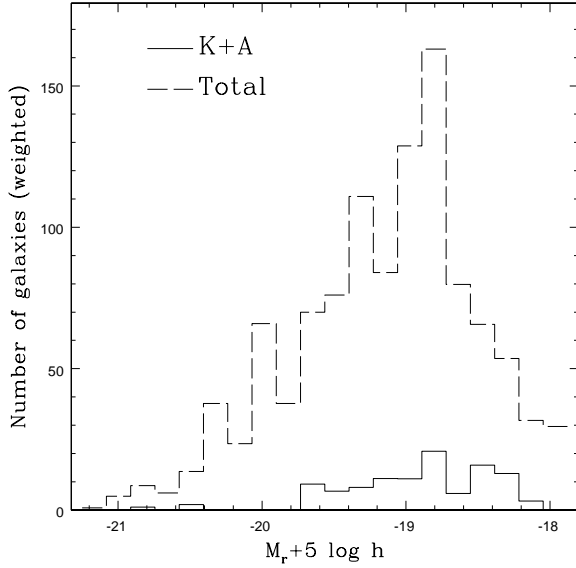


FIG. 18.— The k- and evolution-corrected absolute magnitude distribution for the K+A galaxies (*solid line*) and the full maximal sample (*dashed line*). Many of the K+A galaxies are less luminous than $M_r = -18.8 + 5 \log h$, where the statistical corrections are large and the maximal sample is not representative of a complete photometric sample; the abundance of K+A galaxies is therefore sensitive to the magnitude limit and statistical correction used.

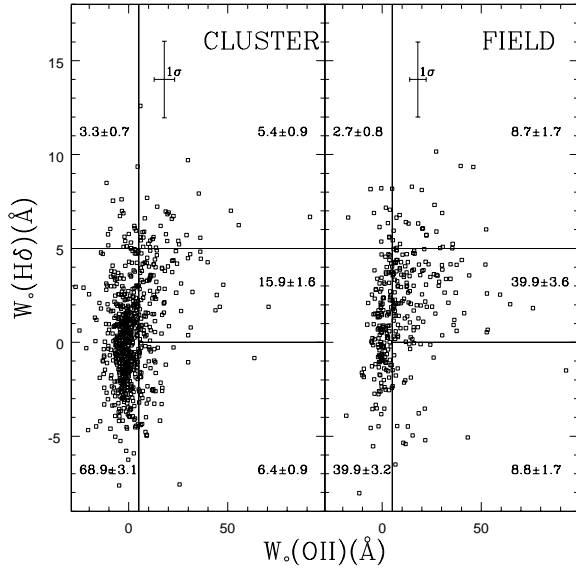


FIG. 19.— The same as Figure 13, but for the luminosity limited sample described in §2.3.2. The fraction of K+A galaxies in the cluster and field samples are equivalent within 1σ uncertainties.

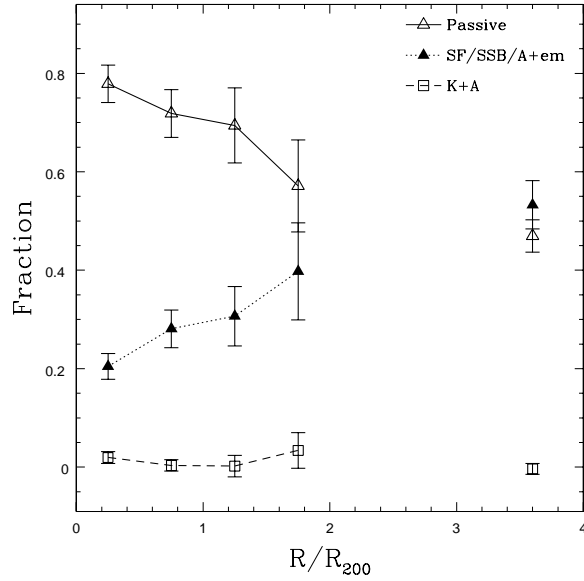


FIG. 20.— The weighted fraction of each type of galaxy, as selected based on its position in the $W_{\odot}(OII)$ - $W_{\odot}(H\delta)$ plane shown in Figure 13, as a function of projected radius. The fractions and 1σ error bars are corrected for the systematic effects of nonuniform scatter, as discussed in §4.2.1. The connected points represent the cluster sample; the isolated points at $R/R_{200} = 3.6$ represent the values in the field sample, plotted at an arbitrary radius for display purposes only.

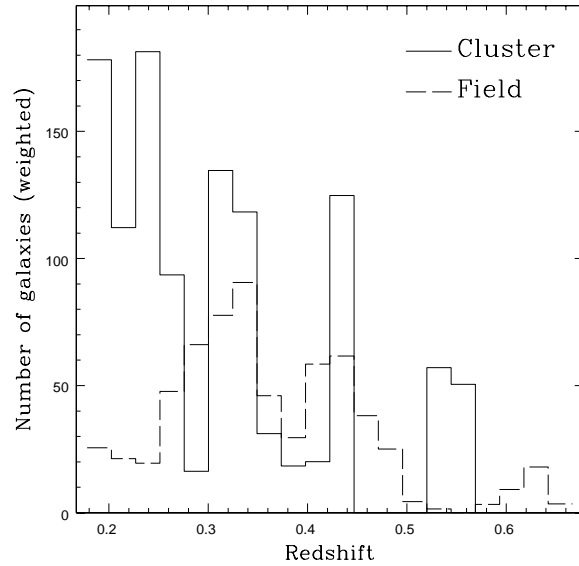


FIG. 21.— The redshift distribution of the cluster (solid line) and field (dashed line) samples, limited to galaxies more luminous than $M_r = -18.8 + 5 \log h$ (corrected for band shifting and evolution).

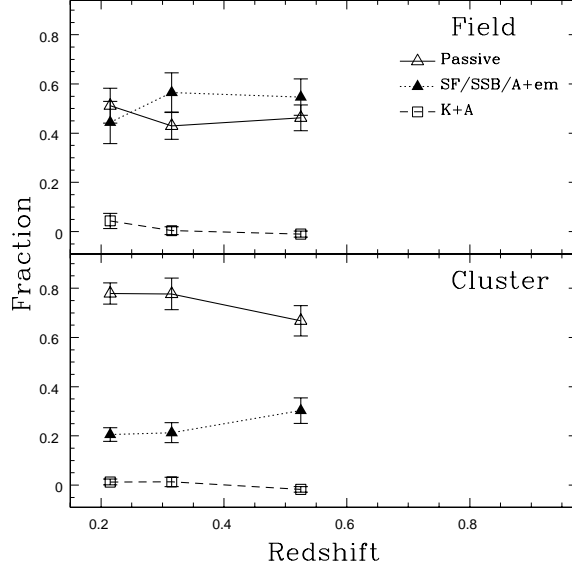


FIG. 22.— This figure shows the fraction of each galaxy population defined in §3.2 and Figure 13, as a function of redshift. Only galaxies more luminous than $M_r = -18.8 + 5 \log h$ are considered. The field galaxy sample is shown in the *top panel*, and the cluster sample in the *bottom panel*. The statistically weighted data are corrected for the systematic effects of scatter in the $W_o(H\delta)$ – $W_o(OII)$ plane, as discussed in §4.2.1. All error bars are 1σ . The K+A fraction is low in all three redshift bins.

different from the field (c.f. Figure 19). Thus, even considering galaxies which may be in the infall regions of clusters, we do not detect evidence for an excess of star forming or K+A galaxies, relative to the field.

4.3. HDS and PSF Fractions

The measurements of $W_o(H\delta)$ and D4000 for the maximal sample (§2.3.3) are shown in Figure 24, for the cluster and field, separately. Each plane is divided into the five regions shown in Figure 11; the number in each panel is the weighted percentage of galaxies within it. The numbers in brackets, for the cluster sample, are from Barger et al. (1996), corrected for small differences in region definitions. We will compare these numbers in §5.2.

We can correct the fraction of galaxies in each region of this figure for the effects of scatter in a manner analogous to the Monte Carlo method described in §4.2.1; the results are shown in Table 4. After this correction, both bHDS (at $1.0 \pm 1.2\%$) and rHDS galaxies ($3.6 \pm 1.4\%$) in clusters are not more common than they are in the field ($2.7 \pm 1.8\%$ and $9.4 \pm 2.2\%$, respectively).

As discussed in §3.3, the HDS galaxies include emission line galaxies; populations with recently truncated star formation should fall into either the PSB or PSF subclasses. In Table 5 we show, for the cluster and field separately, the “raw” PSB and PSF measurement, the estimated scatter correction (assuming that the relative scattered fraction is the same for the PSF/PSB classes as for the rHDS/bHDS classes) and the corrected estimate of the “true” fractions. Again, the fractions of PSB and PSF galaxies are not significantly more common in clusters than they are in the field. In both cases, the PSF galaxies are more abundant,

relative to the PSB galaxies, by a factor of $\sim 5 - 10$. Though this number is quite uncertain, if the large excess is real it may have significant consequences, as we discuss in §6.

4.3.1. Reddening, Metallicity and IMF Effects

A striking feature of Figure 24 is the abundance of galaxies, both cluster and field, with $D4000 \gtrsim 1.9$ and $W_o(H\delta) \gtrsim 2\text{\AA}$, which are not matched by any of the models in Figure 11. This problem has also been pointed out by Couch & Sharples (1987), Morris et al. (1998) and Poggianti & Barbaro (1996), among others, and persists if photometric colors are considered instead of D4000. The problem has been substantially alleviated by considering the narrower D4000 index, but it still persists.

In Figure 25, we plot only the data with $S/N > 15$ and uncontaminated by bright night sky lines near the $W_o(H\delta)$ and $W_o(OII)$ indices. For reference, we plot the initial burst, Salpeter IMF model shown in Figure 11, with a solid line. Using the *deredden* task within IRAF, we redden this model by a large amount, $E_{B-V} = 0.5$; this moves the model to the right by about 0.15, as represented by the dotted line. This reddened model extends in D4000 nearly to the full extent of the data, and the scatter in $W_o(H\delta)$ at the red end is fairly uniform about it.

We also consider two other model variations. The short-dashed line in Figure 25 represents an initial burst model for a galaxy with super-solar metallicity, $Z=2.5Z_\odot$, generated from the updated Bruzual & Charlot (1993) models. Although this model does indeed extend to very

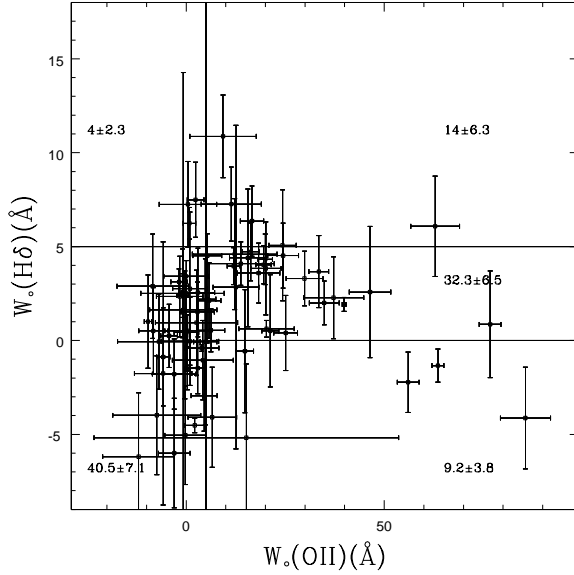


FIG. 23.— Selected from the luminosity limited sample, we show the near-field galaxy population, which has velocities intermediate between our cluster and field definitions, in the $W_o(OII)$ - $W_o(H\delta)$ plane, with 1σ error bars. The regions are the same as in Figure 9, and the number shown in each region represents the weighted percentage of galaxies within that region. The error is estimated assuming Poisson statistics. The fraction of galaxies in each class is not significantly different from the field values shown in Figure 19.

TABLE 4
SYSTEMATIC ERROR ESTIMATIONS IN THE D4000- $W_o(H\delta)$ PLANE

Object Type	Cluster (%)			Field (%)		
	Measured	Scatter	Corrected	Measured	Scatter	Corrected
bHDS	4.7 ± 0.8	3.7 ± 0.9	1.0 ± 1.2	7.2 ± 1.3	4.5 ± 1.3	2.7 ± 1.8
rHDS	9.7 ± 1.0	6.1 ± 1.0	3.6 ± 1.4	11.1 ± 1.8	1.7 ± 1.3	9.4 ± 2.2
SF	10.5 ± 1.1	-12.1 ± 1.1	22.6 ± 1.5	32.7 ± 3.0	-11.3 ± 2.2	44.0 ± 3.7
Passive	73.5 ± 2.8	-0.8 ± 1.2	74.3 ± 3.0	44.7 ± 3.1	1.7 ± 1.6	43.0 ± 3.5
SSB	1.5 ± 0.4	3.1 ± 0.7	-1.6 ± 0.8	6.3 ± 1.5	3.2 ± 1.4	3.1 ± 2.0

TABLE 5
ABUNDANCES OF PSB AND PSF GALAXIES

Object Type	Cluster (%)			Field (%)		
	Measured	Scatter	Corrected	Measured	Scatter	Corrected
PSB	1.3 ± 0.4	1.0 ± 0.2	0.3 ± 0.4	0.7 ± 0.3	0.4 ± 0.1	0.3 ± 0.3
PSF	4.9 ± 0.6	3.0 ± 0.5	1.9 ± 0.8	3.6 ± 0.9	0.5 ± 0.5	3.1 ± 1.0

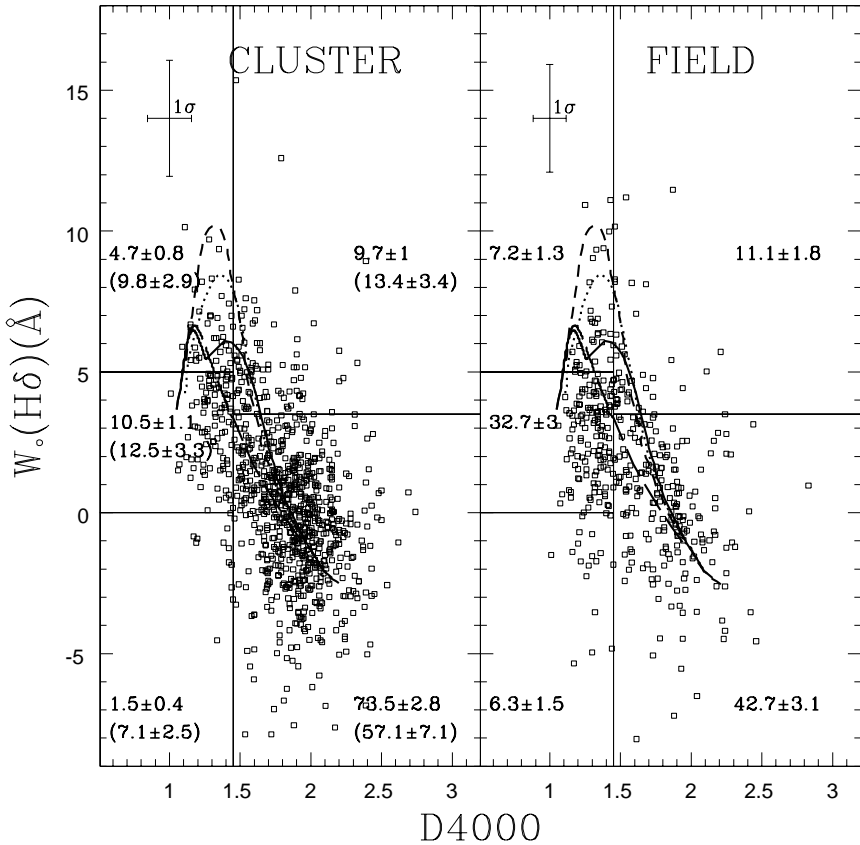


FIG. 24.— The data presented in the D4000- $W_o(H\delta)$ plane, divided into a field and cluster sample. The models and region delineations over-plotted are the same ones shown in Figure 11. The number in each region is the weighted percentage of galaxies in that region, and the errors assume Poisson statistics. The numbers in brackets, for the cluster sample, are from Barger et al. (1996), corrected for the small differences in region definitions. Our results are compared with those of Barger et al. in §5.2. The sample error bars represent the mean 1σ error.

large D4000, the $W_o(H\delta)$ index is always negative¹¹ for $D4000 > 1.9$ and, thus, lies below the bulk of the data. Secondly, we consider the effects of an extreme IMF model, after Rieke et al. (1993), in which no stars less massive than $2M_\odot$ are formed. An initial burst of star formation with this IMF is shown in Figure 25 as the long-dashed line. This model is also able to match the strongest $W_o(H\delta)$ indices of our data with $D4000 > 1.9$. However, the stellar population resulting from such a burst is very short lived, about 300 Myr; thus, it is unlikely that many of these red galaxies can be undergoing such a burst, and we expect that significant dust reddening is the best explanation of the data. This supports the finding of Poggianti et al. (1999), that dust obscuration in galaxies at these redshifts plays an important role in the appearance of their spectra.

5. COMPARISON WITH PREVIOUS WORK

5.1. The Low Redshift Universe

The Las Campanas Redshift Survey (LCRS), as presented in Zabludoff et al. (1996), is a large ($\sim 24,000$ galaxies), unbiased sample of relatively nearby galaxies ($0.05 < z < 0.13$) for which good quality spectra and line indices are available. Zabludoff et al. identify 21 of their 11,113 galaxy subsample ($M_r \gtrsim -19 + 5 \log h$) as E+A (renamed here K+A) types, based on $W_o(OII)$ and an average equivalent width of $H\delta$, $H\gamma$, and $H\beta$ ($< H\delta\gamma\beta >$). They estimate that 1785 galaxies in their sample lie within the infall radius of a rich cluster, and five of these are identified as K+A types; therefore, $0.28 \pm 0.12\%$ of the cluster population are K+A galaxies, compared with $0.17 \pm 0.04\%$ in the field. These fractions are equivalent within 1σ uncertainties. The definition of a K+A galaxy adopted by Zabludoff et al. differs slightly from the one we have adopted here (§3.2) in two respects. First, they use a minimum Balmer index of $< H\delta\gamma\beta > = 5.5 \text{ \AA}$. From the PE-GASE models we find that, for $W_o(H\delta) \approx 5 \text{ \AA}$, $< H\delta\gamma\beta > - W_o(H\delta) \approx 0.7$; thus, our limit of $W_o(H\delta) > 5 \text{ \AA}$ is nearly equivalent to theirs. Secondly, Zabludoff et al. require $W_o(OII) < 2.5 \text{ \AA}$; our lower S/N requires us to use a more generous definition of $W_o(OII) < 5 \text{ \AA}$. Adjusting for this difference allows the inclusion of an additional ~ 13 K+A galaxies in the LCRS sample, raising the total K+A fraction to $0.30 \pm 0.05\%$. Since the uncertainties on the LCRS line indices are small (due to the high S/N of the data), a scatter correction like the one discussed in §4.2.1 is not made.

In our luminosity limited sample (§2.3.2), which most closely matches the luminosity range of the Zabludoff et al. sample, the “raw” K+A fraction in the field is $2.7 \pm 0.8\%$, which we regard as an upper limit. Our best estimate of this fraction, corrected for scatter using the Gaussian cloud method (§4.2.1), is $1.2 \pm 0.8\%$. Thus, the evolution in the K+A fraction over this fairly small redshift range (from $z \sim 0.1$ to $z \sim 0.3$) amounts to a factor of only about 4 ± 2.7 , and the two fractions are actually consistent at about the 1σ level.

5.2. Couch & Sharples (1987) and Related Work

Much of the original work in this field was done by Couch & Sharples (1987), whose dataset of 152 galaxies more luminous than about $M_r = -20 + 5 \log h$ in three clusters at $z \approx 0.31$ was later analyzed in more detail by Barger et al. (1996). As shown in Figure 24, we find somewhat fewer rHDS and bHDS galaxies than Barger et al., though the difference is significant at less than the 2σ level, and may be partly due to an imprecise mapping of $B-R$ to D4000 (which was determined in §3.3). Barger et al. performed a useful and detailed analysis of the distribution of galaxies in this figure, and compared it with model simulations to determine the importance of starbursts to cluster galaxy evolution. They suggest the data are well represented by a model in which $\sim 30\%$ of cluster galaxies have undergone a 0.1 Gyr starburst (which produces 10–20% of the the galaxy’s final stellar mass) in the last ~ 2 Gyr. Given the small number of galaxies and the considerable uncertainties on the line indices, these numbers are uncertain, as the authors acknowledge. In §6 we will argue from the fraction of K+A galaxies in the CNOC1 sample that the importance of such short-lived starbursts in clusters is unlikely to be this large.

The Couch & Sharples data are also considered by Poggianti & Barbaro (1996), who conclude from their modeling that strong starbursts are required to match the K+A galaxies in that sample. However, the comparison between the data and models may be compromised by a difference in index definition. The Couch & Sharples data have $W_o(H\delta)$ indices as large as 9 \AA , with many points around $5 < W_o(H\delta) < 6 \text{ \AA}$, while the post-starburst models of Poggianti & Barbaro struggle to reach $W_o(H\delta) = 6 \text{ \AA}$ (see their fig. 4), and then only for short periods of time. By dividing the data and models into broad categories (i.e. $W_o(H\delta) > 3$ and $(B-R) < 2$) it is possible to misinterpret the results if the models do not match the data *within* a given category, as may be the case here.

5.3. Cl1358+62 and CFRS

Fisher et al. (1998) analyzed spectra for 232 galaxies within a ~ 4 Mpc region around the $z \approx 0.32$ cluster Cl 1358+6245, with a magnitude limit of $M_r \approx -19.1 + 5 \log h$. This improves on the preliminary work presented by Fabricant et al. (1991), which used only 70 spectra in the central regions of this cluster. These authors define K+A (which they term E+A) galaxies in a manner similar to Zabludoff et al. (1996), but with more generous limits in $< H\delta\gamma\beta >$ and $W_o(OII)$. They find 11 ($4.7 \pm 1.9\%$) of their cluster galaxies show K+A type spectra, remarkably similar to our total cluster fraction, before the necessary scatter correction. Since their uncertainties are also comparable to ours, we expect this correction also to be similar, resulting in a reduced, true K+A fraction.

A similar comparison can be made with the work of Hammer et al. (1997), who find a K+A fraction of $4.9 \pm 1.5\%$ in the CFRS field galaxy sample, with a less precise K+A definition, roughly similar to that of Fisher et al. Again, this number should be reduced due to the overestimation resulting from unequal scatter and, thus, the amount of evolution implied relative to the low redshift (LCRS) sample will be significantly less than the order of magnitude implied by the raw fraction alone. This

¹¹Recall, from §2.2, that a negative $W_o(H\delta)$ index does not necessarily imply an emission feature.

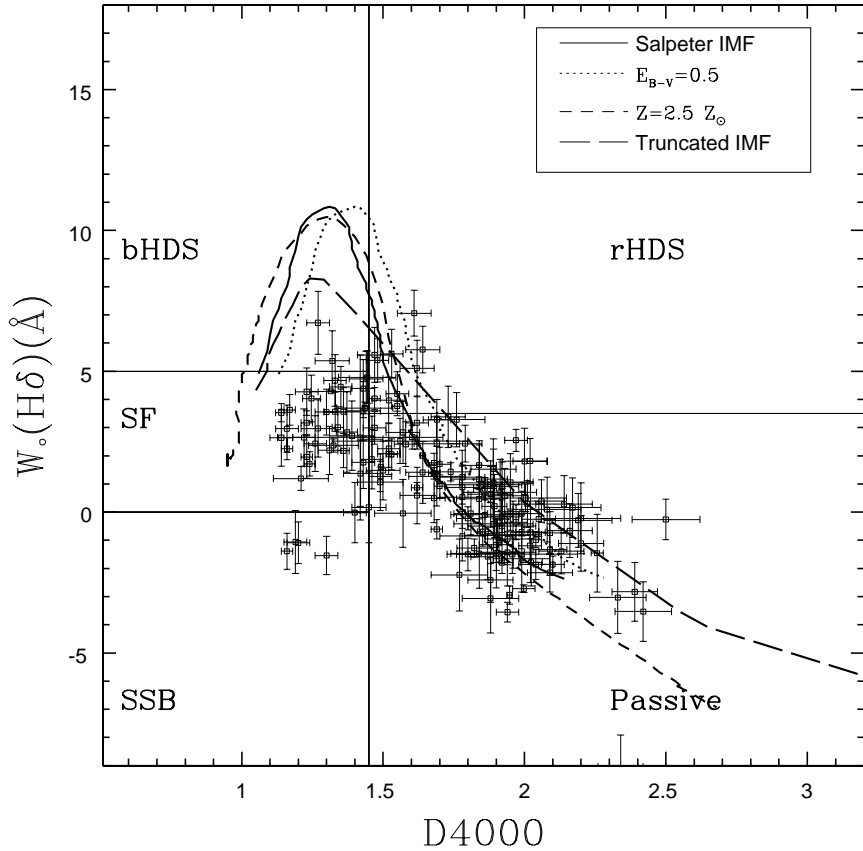


FIG. 25.— PEGASE star formation models presented in the D4000– $W_o(H\delta)$ plane, with regions delineated as in Figure 11. The *solid line* is the standard, Salpeter IMF initial burst model, also shown in Figure 11. This model, reddened by $E_{B-V}=0.5$, is shown as the *dotted line*. A truncated IMF initial burst (Rieke et al. 1993) is shown as the *long-dashed line*, and a high metallicity (GISSEL96) model is the *short-dashed line*. The data plotted are only those with high signal-to-noise ratios ($S/N > 15$) and uncontaminated by bright night sky lines; the error bars are 1σ .

number is similar to our raw cluster K+A fraction, but somewhat larger than our field value. Thus, it supports our conclusion that K+A galaxies are not preferentially found in clusters; however, we note that the mean redshift of the CFRS, $z \approx 0.6$, is considerably higher than that of the CNOC1 sample, and evolutionary effects may be important.

5.4. The MORPHS Collaboration

After this paper was submitted, the MORPHS collaboration published a similar study based on ten clusters at $0.37 < z < 0.56$, including 657 galaxies brighter than $M_r \approx -19 + 5 \log h$. (Dressler et al. 1999; Poggianti et al. 1999). These authors conclude that galaxies without detectable [O II] emission but $W_o(H\delta) > 3 \text{ \AA}$ (which they call k+a/a+k) are significantly more common in the cluster sample than the field, ($21 \pm 2\%$ compared with $6 \pm 3\%$). Both the largeness of these fractions, and the significance of their difference, are apparently in conflict with the results we have presented in §4.2. This difference warrants a detailed comparison of the data and analysis, which we present in this subsection.

We will first show that our data are of comparable quality to the MORPHS data, and then suggest that the differences in our conclusions may result from (1) different selection criteria (both of galaxies and of clusters); (2) different treatment of uncertainties; and (3) differences in galaxy classifications and definitions.

5.4.1. A Comparison of Data Quality

We have obtained the publicly available MORPHS data from <http://www.ociw/~irs>, and computed our indices from their data directly. However, the MORPHS data do not include error vectors, and uncertainty estimates of their indices are unpublished; thus care must be taken before quantitative comparisons are made with our results. In particular, continuum S/N ratios cannot be computed in the same way as we have done in §2.1. Instead, we define an alternate estimate as the mean flux per pixel divided by the *r.m.s.* in the wavelength region $4050 < \lambda/\text{\AA} < 4250$. This underestimates the true S/N, especially for high S/N spectra, due to real features in the spectrum. In Figure 26 we show how this “alternate” value of S/N, computed for the CNOC1 galaxies, compares with our definition in §2.1. The correlation is evident, though the scatter is large, and the underestimation of S/N at high S/N values is clear. Based on this correlation, we will assume that our alternative definition can hold as a reasonable proxy for the more realistic measurement used to qualify the CNOC1 data.

In Figure 27, we compare the S/N distribution of the CNOC1 sample to that of the MORPHS sample (excluding from the latter galaxies that have a quality index of 4, which are defined as those with S/N sufficient only for a redshift determination). In both cases, S/N is computed in the “alternative” manner described above. Both samples have similar distributions, apart from a small excess of low S/N objects in the MORPHS sample¹². We can crudely assign an uncertainty to the index measurements

made on the MORPHS sample by correlating the errors on the CNOC1 data with our alternative S/N measurement. From the S/N measured on the MORPHS data, we can then determine approximate index uncertainties. Representing the uncertainties in $W_o(H\delta)$ and $W_o(OII)$ by $\Delta H\delta$ and $\Delta[\text{O II}]$, respectively, we find $\Delta H\delta = 9.2 \times (S/N)^{-1.08}$ and $\Delta[\text{O II}] = 32.8 \times (S/N)^{-1.22}$.

The uncertainty of a line index will be reduced if the resolution is improved, and the continuum S/N ratio is fixed. The MORPHS spectra were obtained using different telescopes and instruments, and are not all of the same resolution; the best resolution spectra (obtained with the COSMIC spectrograph) have a dispersion of 3.1 \AA per pixel, and are smoothed to the instrumental resolution of $\sim 8 \text{ \AA}$, and rebinned to 10 \AA per pixel. Thus, the average FWHM of emission lines is comparable to that of the CNOC1 spectra, $\sim 16.5 \text{ \AA}$, as confirmed by the measurement of several [O II] lines.

A second property which must be tested is the equivalence of the CNOC1 line indices to those measured by the MORPHS collaboration. In Figure 28 we show the values of our $W_o(H\delta)$ index, defined in §2.2 and measured on the MORPHS spectra, compared with those of Dressler et al. (1999). We exclude galaxies with quality indices of 4, or flagged as uncertain. The latter were usually computed by interactively fitting the continuum and then fitting a Gaussian profile to the absorption or emission lines. Given the noisy nature of the data, and the generally complex region of the spectrum under consideration, we find that such an interactive approach is difficult to duplicate, and makes uncertainty estimates difficult to determine reliably. Nonetheless, the correlation between our $H\delta$ index and that of Dressler et al. is fairly good. In particular, we recover the large $W_o(H\delta)$ indices measured in many cases by Dressler et al., showing that our index is not insensitive to spectra of this type. The scatter in this figure reflects the fact that both of these indices have considerable uncertainties.

5.4.2. Reanalysis of MORPHS Data

In Figure 29 we show the MORPHS data in the $W_o(OII)$ - $W_o(H\delta)$ plane, with our region delineations from §3.2, and the measurements we have made using our index definitions (§2.2). We exclude data of quality index 4, and mark as open circles those galaxies which are either flagged as having uncertain $W_o(H\delta)$ measurements, or for which no $W_o(H\delta)$ measurement is listed in the MORPHS catalogue (i.e., they are listed as either INDEF, or 0). Furthermore, no magnitude limit is imposed. The sample error bars represent the mean error in each index. The field sample is somewhat biased to lower S/N galaxies and, hence, results in larger mean index errors.

We will not attempt to evaluate the fractions of each type of galaxy (K+A, SF etc.) that we have defined for galaxies in this plane, due to the difficulty in correcting for the morphologically based selection (see Smail et al. 1997). There is clearly, however, a strong presence of K+A galaxies in the cluster sample that is not observed in the field. For most (20/24) of the galaxies with $W_o(H\delta) > 10 \text{ \AA}$,

¹²These S/N ratios are computed *per pixel*, and the CNOC1 spectra are sampled at 3.45 \AA per pixel, while many of the MORPHS spectra are more coarsely sampled (for example, the COSMIC spectra are rebinned to 10 \AA per pixel).

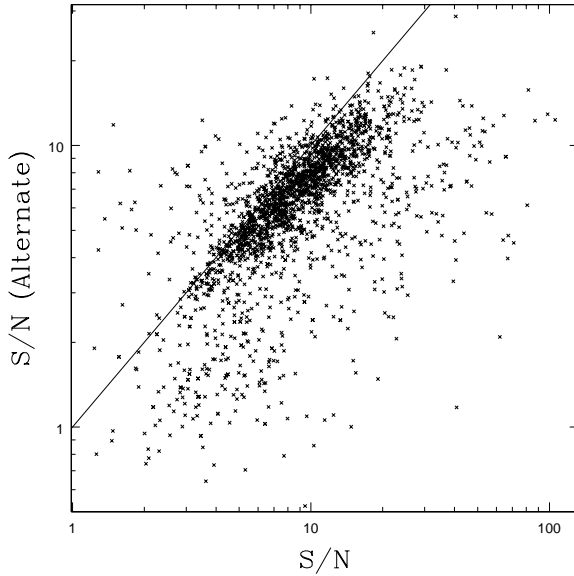


FIG. 26.— Using the CNOC1 sample, we compare the S/N measured in the manner defined in § 2.1 (on the x-axis) to the alternate definition described in § 5.4.1. The *solid line*, drawn for reference, is where the points would like if both S/N measurements were equal. Most of the data show a strong correlation, though there is significant scatter. The alternate definition underestimates the S/N, especially at high values, where real features in the continuum add to the *r.m.s.* which is used instead of the noise.

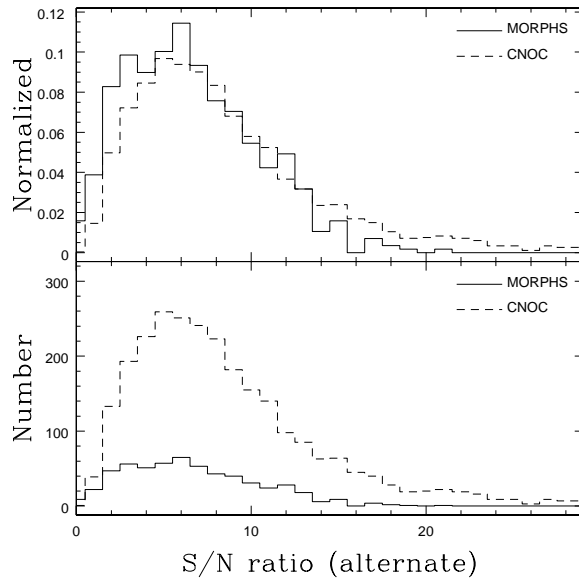


FIG. 27.— We compare the S/N distribution for galaxies in the MORPHS sample with quality indices less than 4 (*solid line*) to that in the CNOC1 sample (*dashed line*). In this case, S/N is measured as the ratio of the mean flux per pixel in the range $4050 < \lambda/\text{\AA} < 4250$ to the *r.m.s.* in the same range. The *bottom panel* shows the number of galaxies in each bin; in the *top panel* both samples are normalized to unit area.

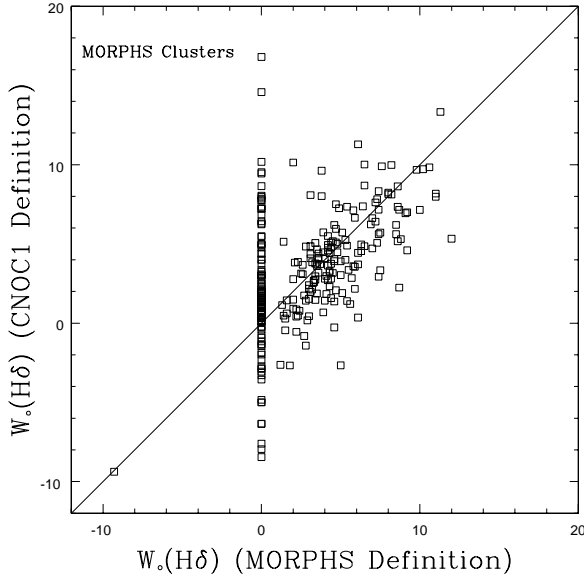


FIG. 28.— Our measurements of $W_o(H\delta)$ for galaxies in the MORPHS galaxy sample (on the y-axis) are compared with the equivalent widths published in Dressler et al. (1999, on the x-axis), excluding galaxies with low quality indices ($q = 4$) or flagged as uncertain in the catalogues. Although the two indices are defined in very different ways, they are correlated. The *solid line* shows where the two indices are equal; it is not a fit to the data. The scatter in this figure reflects the uncertainty in both indices, which arises from low S/N data and uncertainty in continuum placement.

Dressler et al. (1999) either did not measure $W_o(H\delta)$ or the measurement was flagged as uncertain (open circles). Often, this is due to poor sky subtraction near the line, which should result in large index uncertainties that justify their removal from the sample (as we do for our maximal sample in §2.3.3). However a large population of cluster K+A galaxies with $W_o(H\delta) < 10\text{\AA}$ persists. This strong population is clearly not as abundant in the MORPHS field sample, in contrast with the results found in our sample (Figure 13). Due to the unusual selection criteria, however, the absolute fraction of K+A galaxies in the two samples cannot be easily compared in a quantitative way.

5.4.3. Possible Sources of Differences Between MORPHS and CNOC1

Given that the CNOC1 resolution, S/N distribution and line index definitions are comparable to those of the MORPHS collaboration, what is the source for the difference in results? We discuss three possibilities below.

Cluster Selection: Given that galaxy clusters are a very heterogeneous class of objects, with differing galaxy populations, some or all of the difference between the MORPHS and CNOC1 results may be in cluster selection. The CNOC1 clusters are among the most X-ray luminous at these redshifts, often containing cooling flows, and are mostly dynamically relaxed (Lewis et al. 1999). It is quite possible that, as a class, these clusters differ from the more heterogeneously selected clusters in the MORPHS sample (though we confirm K+A fractions of $\lesssim 5\%$ for the two clusters in common with both samples). Furthermore, the MORPHS clusters are generally at higher redshifts than

the CNOC1 targets; all but four of the CNOC1 clusters lie at redshifts less than that of the lowest redshift MORPHS cluster, A370.

Galaxy Selection: The selection of spectroscopic targets from the photometric sample differs in the two surveys. The MORPHS sample was primarily selected based on galaxy morphology; Sd/Irregular galaxies are oversampled relative to earlier types. Since late-type galaxies were targeted preferentially, the detection of a large population of starburst and/or post-starburst galaxies may not be surprising. Dressler et al. (1999) attempt to correct for this by comparing the morphological distribution of their spectroscopic sample with the photometric sample, but this correction is not completely reliable since the statistical correction for late type field galaxies is uncertain (Smail et al. 1997). Alternatively, the primary selection criterion in the CNOC1 sample is apparent magnitude, with small corrections for galaxy color and position. In particular, we note that any color selection effect is quite small, and there does not seem to be a significant bias to our results as a function of galaxy spectral type at these apparent magnitudes. As discussed in section 2.3.1, we used weighting functions to correct our sample of line indices to be representative of the full photometric sample in the cluster fields.

We also note that the CNOC1 survey includes galaxies at much larger distances from the cluster center, as shown in Figure 30. However, the lack of an observable gradient in the K+A fraction (Figure 22) makes it unlikely that this can have a strong effect.

Uncertainties: No uncertainties are published for the line indices presented in Dressler et al. (1999) or Poggianti

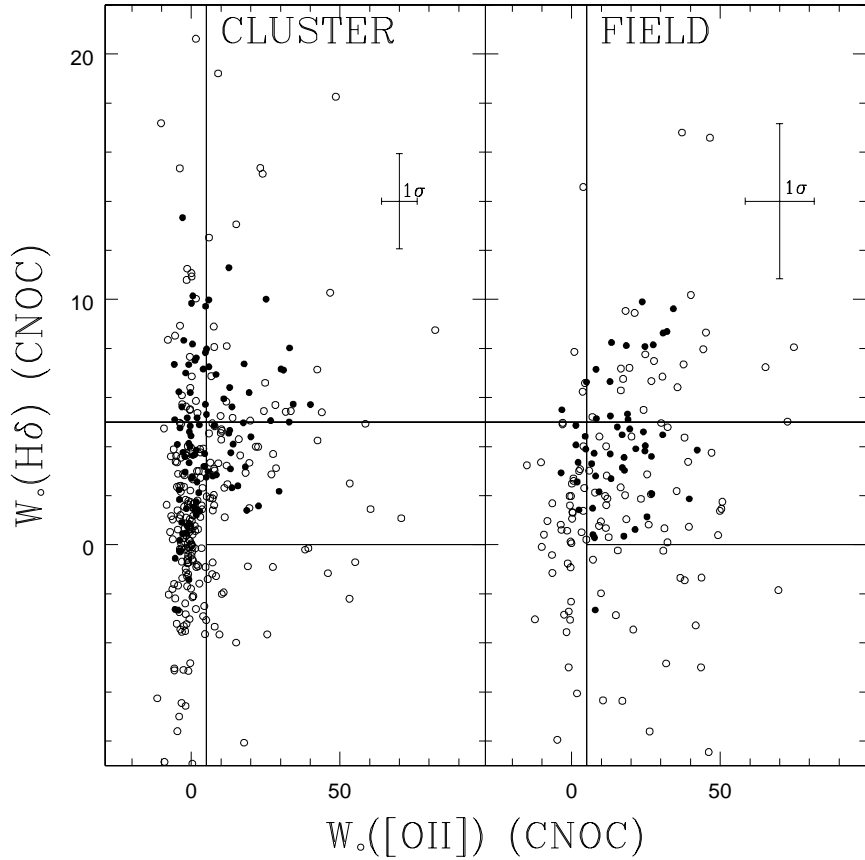


FIG. 29.— Our measurements of $W_o(OII)$ and $W_o(H\delta)$ on the MORPHS cluster and field samples. Data which are of quality index 4 have been excluded. *Open circles* are data for which either no $W_o(H\delta)$ measurement is presented in the MORPHS catalogue, or the measurement is flagged as uncertain. The sample error bars represent the mean, 1σ uncertainty, computed assuming the CNOC1 correlation between S/N and index uncertainty holds for the MORPHS sample. This figure may be compared with the CNOC1 data presented in Figure 13, but note that the selection criteria are different in that the MORPHS data are biased toward late type galaxies (which will generally have stronger $W_o(OII)$ and $W_o(H\delta)$ indices). There is a clear excess of K+A galaxies in the MORPHS clusters, relative to their field sample. Although the absolute fraction of K+A galaxies in this sample is difficult to determine reliably, this excess suggests that the MORPHS clusters may have different galaxy populations than the X-ray luminous clusters considered in the present work.

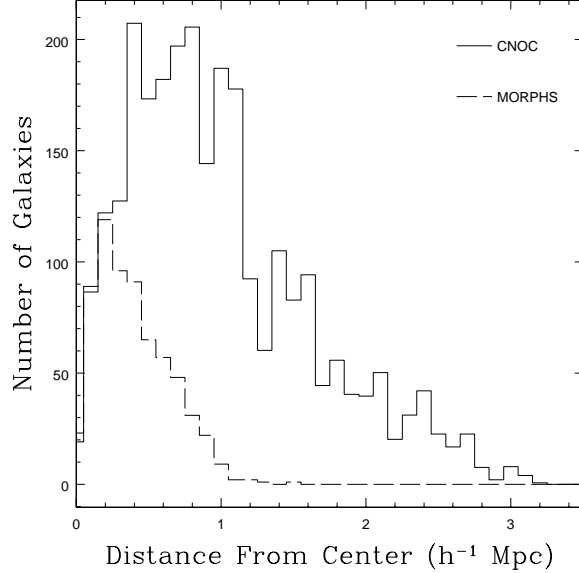


FIG. 30.— The distribution of distances from cluster centers, for galaxies in the CNOC1 (*solid line*) and MORPHS (*dashed line*) samples. The CNOC1 distribution is weighted by W_{spec} (see §2.3.1), but renormalized so that the total number of galaxies represented in this figure corresponds to the number in the spectroscopic sample. On average, galaxies in the CNOC1 sample come from radii about 3 times larger than galaxies in the MORPHS sample.

et al. (1999). As we have shown in § 4.2.1, the large uncertainties of our indices result in an overestimate of the K+A fraction; since we believe the MORPHS index uncertainties to be comparable to ours, the same holds true for their sample, and some correction for this effect must be made. Index measurements for galaxies with undetectable or hard to measure lines are not listed in Dressler et al. and, thus, the scatter in the measurements that do exist does not accurately reflect the average uncertainty of the data.

Galaxy Classifications: Based on unpublished recomputations of the Barbaro & Poggianti (1996) models, using their new $W_o(H\delta)$ definition, Poggianti et al. (1999) have chosen a threshold of $W_o(H\delta) > 3 \text{ \AA}$ for their classification of k+a/a+k galaxies. This is considerably lower than we have adopted for our K+A definition, and clearly leads to the identification of a larger population of “unusual” galaxies. We have justified our limit not only by comparison with the PEGASE models, but also by comparison with the local data of Kennicutt et al. (1992a) and Kinney et al. (1996). From Figure 9 alone, it is clear that galaxies with $W_o(H\delta) > 3 \text{ \AA}$ and no detectable [O II] emission are *not* exclusively K+As, but include normal S0 and early spiral galaxies. Since the Dressler et al. $W_o(H\delta)$ threshold is significantly lower than previously adopted by many other authors (e.g., Dressler & Gunn 1983, Fabricant et al. 1991, Zabludoff et al. 1996, Abraham et al. 1996, Morris et al. 1998), we chose not to adopt their lower limit. Adopting 3\AA instead of 5\AA as our lower limit for the classification of K+A galaxies would increase the fraction of galaxies that satisfy this definition¹³. To some

extent, of course, the choice of limiting $W_o(H\delta)$ is quite arbitrary and of little consequence as long as it is interpreted as such, and accounted for when comparisons with other work is made.

5.5. Summary

With the exception of the MORPHS results (Dressler et al. 1999), the surveys discussed above are not inconsistent with our principal results, which are: (1) the fraction of K+A galaxies (as defined in §3.2) in the field and X-ray luminous clusters at $z \approx 0.3$ is less than 5%; (2) it has not been shown conclusively that the $z \approx 0.3$ K+A fraction is significantly larger than the fraction at $z \approx 0.1$; and (3) there is no strong evidence yet that K+A galaxies are more common in cluster environments than in the field. We suggest that the higher fractions of K+A galaxies found by the MORPHS group may come from the very different methodologies used, especially in the selection of the galaxy sample. We suggest that the simpler CNOC1 sample and weighting functions are likely to produce a fair sampling of the cluster populations. In addition, there may be an actual difference in the populations of our two differently selected cluster samples. In that case, it remains to be seen whether clusters at these redshifts are better typified by the X-ray luminous CNOC1 sample, or the more heterogeneous MORPHS sample.

6. DISCUSSION

It was shown in Balogh et al. (1997) that the star formation rate (determined from [O II] emission lines) at all

¹³For reference, $7.6 \pm 1.1\%$ of cluster galaxies, and $9.1 \pm 1.6\%$ of field galaxies in our luminosity limit sample have $W_o(H\delta) > 3 \text{ \AA}$, and $W_o(OII) < 5 \text{ \AA}$ (uncorrected for scatter).

radii within CNOC1 clusters is always less than that in the field galaxy population. However, if a substantial fraction of cluster galaxies have undergone massive but very short starbursts, as postulated for example by Barger et al. (1996), the short duration of these bursts (≈ 100 Myr) would mean that only a small fraction of cluster galaxies would be observed in the burst phase at a given epoch.

According to the results of the PEGASE models, following a short burst a galaxy will appear as a PSB or PSF type for between 0.75 and 1 Gyr. Thus, the starburst rate can be determined from the abundance of these “remnants”. For our maximal sample (§2.3.3), the fraction of these galaxies in the cluster is less than $6.2 \pm 0.7\%$; this is an upper limit because it does not include the correction for non-uniform scatter. This implies that, in the last 2 Gyr, less than approximately $15 \pm 2\%$ of the galaxy population may have undergone a starburst. Using our best estimate for the scatter correction from Table 5, the corrected fraction of cluster PSB and PSF galaxies is $2.2 \pm 0.9\%$, which reduces the estimated starburst population to only $\sim 6\%$ in the last 2 Gyr. This is much less than the 30% estimated by Barger et al. (1996). Part of this difference is due to the factor of two difference between the abundance of HDS galaxies in our respective samples, as shown in Figure 24 (significant at the $\sim 2\sigma$ level). Secondly, our fractions are reduced due to the scatter correction, though Barger et al. include their uncertainties in their models, which should account for this effect if their error bars are reliable. Finally, Barger et al. actually model the HDS galaxies (which comprise $4.6 \pm 1.8\%$ of our cluster sample, after scatter correction) with post-starburst tracks; however, some of these have [O II] emission (the A+em galaxies), and cannot therefore be truly post-starburst.

Poggianti et al. (1999) have recently suggested that the A+em galaxies are dusty starbursts which may later evolve into K+A types; the strong Balmer lines arise because the OB-stars responsible for the emission lines are heavily obscured by dust, while the longer lived A stars have migrated out of their birthplaces and are more widespread throughout the galaxy, so that their light dominates the spectrum. In our cluster sample, we find $3.0 \pm 0.9\%$ of the galaxies have A+em spectra, after scatter correction. This is almost two times larger than the K+A galaxy fraction and implies that the A+em phase must last at least twice as long as the K+A phase if the two types are evolutionarily linked, and if *all* A+em galaxies evolve into K+A types. Thus, these dusty starbursts should either be fairly long-lived, with lifetimes of more than 1.5 Gyr, or a large fraction of them never evolve into K+A types. The fraction of field galaxies classified A+em, $6.3 \pm 2.1\%$, is twice as large as the cluster fraction. Thus, the cluster environment does not appear to be responsible for preferentially generating these galaxy types, whether or not they are starbursts. It is also possible that, if this interpretation of A+em spectra is correct, some K+A galaxies are just a more extreme example, in which the [OII] $\lambda 3727$ line is completely obscured, as pointed out by Poggianti et al. In this case, A+em and K+A galaxies are not evolutionary counterparts, but representative of the same, starburst phenomenon.

Assuming that K+A galaxies are the result of recently terminated star formation, we can use the fractions of PSF

and PSB galaxies in our sample to assess the relative contribution of starbursts and truncated star formation to this scenario. In general, PEGASE models of post-starburst galaxies spend roughly an equal amount of time in both PSB and PSF stages, while truncated star formation leads only to PSF galaxies, lasting about 300 Myr after the star formation activity ceases (see §3.3). Thus, if starbursts are the dominant mechanism for generating HDS galaxies, there should be (roughly) an equal number of PSB and PSF galaxies. As shown in §4.3, the PSF fraction in both cluster and field environments may be much higher ($\sim 5 - 10$ times) than the PSB fraction. If this overabundance is real, it suggests that at least some of the galaxies may have had their star formation truncated without a burst, as supported, for example, by recent simulations (Fujita et al. 1999).

The lack of a marked excess of K+A or A+em galaxies relative to the field may suggest that the cluster environment does not actively truncate *or* induce star formation, but merely inhibits it from regenerating once it has ceased. For example, in the galaxy formation model of Baugh, Cole & Frenk (1996), after a merger of two spiral galaxies succeeds in producing an elliptical galaxy, halo material may recollapse to form a new disk. This reformation of a stable disk could conceivably be inhibited in the cluster environment, due to the presence of strong tidal fields and galaxy harassment. Furthermore, the halo of gas surrounding a spiral galaxy, which may continually cool onto the disk, forming new stars, may be easily stripped away when a galaxy falls into a cluster (Larson, Tinsley & Caldwell 1980). The conditions for this to happen are much less stringent than those for stripping all the gas out of the galactic disk. In either of these cases, K+A galaxies will generally evolve to become Passive within the cluster once they have exhausted their gas supply, whereas, in the field, many will again become star-forming galaxies. Starbursts and K+A phases are then interpreted as natural stages in galaxy evolution (i.e., galaxies form stars in bursts, not continuously), and the cluster merely prevents a galaxy from recommencing its star formation once the activity has stopped of its own accord. We are currently analyzing dark matter simulations of clusters to link a galaxy’s star formation history to the time elapsed since it was accreted. Preliminary analysis shows that a gradual reduction of SFR following galaxy accretion adequately reproduces the radial gradient of star formation (Balogh et al., in preparation).

There are several caveats which may alter the conclusions described above, and there are several ways in which future observations may address these issues; we list these caveats below:

1. Once statistical correction weights are included, our spectroscopic sample is representative of a photometric sample complete to $M_r = -18.8 + 5 \log h$. When star formation is truncated in the more numerous, faint galaxy population, they will fade and many will drop below this limit. Indeed, the K+A galaxies in our sample appear to be of intrinsically low luminosity. It is also known that the less luminous galaxies evolve more significantly with redshift (Lilly et al. 1995; Lin et al. 1997), and thus contribute more to the Butcher-Oemler effect. Thus, it is possible that

there exists a large number of faint K+A galaxies which we are not detecting, and these may show an environmental preference.

2. Whether or not an equal fraction of K+A galaxies in the cluster and field necessarily implies an equal production rate of starbursts in both environments is somewhat model-dependent, as it may only be a subset of the total population that is ever engaged in starburst activity. For example, the results of Ellis et al. (1997) and Barger et al. (1998) suggest that most cluster ellipticals formed from a single burst many Gyr ago, and have since evolved passively. If we assume that the Passive type galaxies play no part in cluster evolution, then the fraction of “active” galaxies in clusters that have a K+A spectrum is $6 \pm 3\%$, (corrected for scatter effects). However, it is not yet clear how many of the Passive galaxies are safely excluded in this manner; many of our Passive galaxies have spectra consistent with those of early type spirals and S0 galaxies. Furthermore, it is not clear what fraction of the field galaxies are also “primordial” (e.g., Kelson et al. 1997; Kodama et al. 1998).
3. The [OII] index is metallicity dependent, which affects star formation rates derived from its measurement; however, this dependence is fairly weak (Kennicutt 1992a) and unlikely to strongly affect our results. More important is the fact that this blue feature is quite sensitive to dust obscuration, and many of the PSB or PSF galaxies with $W_o(OII) \lesssim 5\text{\AA}$ may have significant, but dust-obscured, star formation (e.g., Poggianti et al. 1999). Infrared spectroscopy and imaging, and measurements of H α emission, will be helpful in constraining this effect.
4. The K+A population is known to be morphologically heterogeneous (Couch et al. 1998; Caldwell, Rose & Dendy 1998). If high resolution HST imaging reveals that K+A galaxies in clusters are morphologically distinct from those in the field, this may support models in which the mechanisms which are responsible for generating K+A galaxies are environment-dependent.
5. Kauffmann (1995) and Andreon & Ettori (1999) have suggested that the X-ray luminous clusters observed at moderate redshifts are not the evolutionary predecessors of the less luminous, low redshift clusters to which they are often compared. In particular, the CNOC1 sample is composed of the most X-ray luminous clusters in the universe and, hence, may have unique or unusual galaxy populations; this may be responsible for some of the discrepancy between our results and those of Dressler et al. (1999). We note, however, that Andreon & Ettori find no dependence of the blue galaxy fraction on X-ray luminosity, specifically.
6. Finally, the field sample drawn from the foreground and background of these rich clusters may be unusual in some way, though results are generally consistent with the field samples of other groups (Lin

et al. 1997). Work is currently being undertaken to address this issue using the CNOC2 field galaxy sample (Ellingson et al., in preparation).

7. SUMMARY AND CONCLUSIONS

We have presented a detailed analysis of the spectral characteristics of a large sample of galaxies in X-ray luminous clusters between $z=0.18$ and $z=0.55$, and of an identically selected field galaxy sample. We focus on three spectral indices: D4000, which traces the old stellar population; $W_o(H\delta)$, which indicates the presence of A-type stars and is sensitive to star formation that took place up to 1 Gyr ago; and the $W_o(OII)$ index, which indicates current star formation activity. We compare our data to the model predictions of Fioc & Rocca-Volmerange (1997) and Bruzual & Charlot (1993), and draw the following conclusions:

- The radial trends within the cluster sample are consistent with a continuous age sequence, in the sense that the last episode of star formation occurred more recently for the outermost galaxies than for the central galaxies.
- We define K+A galaxies as those with $W_o(OII) < 5\text{\AA}$, and $W_o(H\delta) > 5\text{\AA}$. Our measured K+A galaxy fraction is $4.4 \pm 0.7\%$ in the cluster and $1.9 \pm 0.6\%$ in the field, but this is only an upper limit due to the large index errors which tend to overestimate these numbers. Attempting to correct for this effect, we find the true fraction of K+A galaxies to be only $2.1 \pm 0.7\%$ in the cluster environment, and $0.1 \pm 0.7\%$ in the field. For our luminosity limited sample (galaxies brighter than $M_r = -18.8 + 5 \log h$), these corrected values are $1.5 \pm 0.8\%$ (cluster) and $1.2 \pm 0.8\%$ (field). Our field results are consistent with the LCRS $z = 0.1$ fraction of 0.30% (Zabludoff et al. 1996) at the $\sim 1\sigma$ level.
- The fraction of cluster galaxies which are undergoing, or have recently undergone, a short burst of star formation is not significantly greater than the field fraction, at any redshift or distance from the cluster center. From the fraction of PSB and PSF galaxies, we conclude that less than $\sim 10\%$ of the galaxies in both the cluster and the field may have undergone short starbursts in the last 2 Gyr.
- If all the A+em galaxies are dusty starbursts and progenitors of the K+A galaxies, then these must be undergoing fairly long-lived episodes of star formation (> 1.5 Gyr). These galaxies are two times more common in our field sample than in the cluster.
- We find that PSF galaxies may outnumber PSB galaxies by a factor of 5-10, in both cluster and field environments (though the samples are small). Comparison with models suggests that truncated star formation *without* a short starburst phase may play a significant role in galaxy evolution.
- More photometry of the CNOC1 fields is still needed; particularly K-band to constrain the total stellar mass, and U-band to independently measure star

formation rates. Infrared imaging and spectroscopy is needed to determine the amount of dust-obsured star formation, and HST images are required to sub-classify the various galaxies types morphologically.

Keeping in mind the caveats listed at the end of §6, we can discuss some of the implications of our results. The general trend for higher redshift clusters to be bluer (the B–O effect) has not yet been linked to a population of galaxies unique to the cluster environment. The simplest explanation consistent with the current data is that the B–O effect in clusters largely reflects the increased level of star formation in the field at larger redshifts. Secondly, there is no evidence that recent (<1 Gyr) cluster-induced star formation is responsible for driving the differential evolution between cluster and field within the virial radius, since there is no tell-tale population of starburst or post-starburst cluster galaxies that does not exist in the field. We speculate that the presence of bursting galaxies, and

the possible increase of such galaxies with redshift, reflects the general nature of star-forming galaxies, independent of environment. However, galaxies in dense environments are eventually *prevented* from bursting, perhaps because their halo gas reservoir has been stripped. This, coupled with a population of “primordial” ellipticals and perhaps some truncation due to ram pressure stripping of disk gas, could be responsible for the older stellar populations which inhabit cluster environments.

The data used in this paper form part of the CNOC1 study of intermediate-redshift clusters. We are grateful to all the consortium members and to the CFHT staff for their contributions to this project. MLB is supported by a Natural Sciences and Engineering Research Council of Canada (NSERC) research grant to C. J. Pritchett and an NSERC postgraduate scholarship. MLB is grateful to J. F. Navarro and A. Zabludoff for useful discussions.

APPENDIX

A DESCRIPTION OF THE PEGASE MODELS

In this Appendix we will discuss in more detail the PEGASE models shown in Figure 11, on which our galaxy classification system (§3.3) is partly based.

The large, open star in Figure 11 represents the model result for a galaxy with a constant star formation rate, of any intensity. It represents the maximum $H\delta$ absorption one can expect in a normal galaxy; emission filling will reduce its value by between roughly 1 and 3.5Å (Barbaro & Poggianti 1997). This point lies blueward of our D4000 cut, within the SF region. All of the galaxies in the SF region are either spirals, irregulars, or “starburst” galaxies, and do not have $W_o(H\delta)$ stronger than the model constant star-formation point (with the exception of NGC 3034, discussed in §3.2). Only if the star formation activity has begun recently (within the last 200 Myr, Barbaro & Poggianti, 1997) will $H\delta$ emission overwhelm the absorption and the galaxies will then occupy the short starburst (SSB) region of this figure.

The long-dashed line in Figure 11 traces the evolutionary path of a galaxy with an exponentially decaying star formation rate; it evolves from “birth” at $D4000 \approx 1$, redward. In this case, a decay time of $\tau = 2$ Gyr is adopted, and the galaxy is evolved to 11 Gyr, which we expect to be the maximum age of CNOC1 galaxies, in reasonable cosmological models¹⁴. Most of the local spirals in the Kennicutt (1992b) and Kinney et al. (1996) samples lie close to this curve. Galaxies of this type with ages greater than about 5 Gyr will lie in the Passive region; clearly this includes not only E and S0 type galaxies, but also early type spirals. Note that the oldest models have $W_o(H\delta) < 0$; this reflects the nature of our specific index definition, which in this case is telling more about features in the continuum, rather than the intrinsic $H\delta$ absorption (see §2.2).

The evolution of a galaxy produced by an initial burst of star formation lasting 200 Myr is shown as the short-dashed line in Figure 11. After the burst ends, this spectrum always has stronger $W_o(H\delta)$ than the exponentially decaying star-formation model, until $D4000 > 1.7$. It spends roughly 300 Myr in the bHDS region and another 300 Myr in the rHDS region.

The dotted line represents the evolution of a galaxy which underwent constant star formation for 4 Gyr, followed by a 200 Myr starburst involving 30% of its mass, after which all star formation was terminated. This model track only follows the evolution after the end of the starburst. The model closely traces the initial burst model, but does not reach as strong values of $W_o(H\delta)$. The duration and strength of the burst are quite arbitrary; longer bursts and bursts involving smaller amounts of stellar mass result in weaker maximum $W_o(H\delta)$ indices; this parameter space has been explored extensively by Poggianti & Barbaro (1996), though we warn that our $W_o(H\delta)$ indices are defined differently and are not directly comparable with theirs.

The rHDS galaxies can originate not only from a terminated SSB phase, but also from a galaxy in which long-term star formation has recently ended (e.g., Couch & Sharples 1987, Newberry, Boroson & Kirshner 1990). We model this latter case by terminating star formation in a galaxy which has undergone constant star formation for 4 Gyr; this is shown in Figure 11 as the solid line. Once the star formation is terminated, the galaxy quickly reddens, passing into the rHDS region within 100 Myr. It then spends about 300 Myr in the rHDS region before $W_o(H\delta)$ further weakens and the spectrum becomes a Passive type.

¹⁴Beyond an age of 11 Gyr, the models only increase in D4000 at a rate of about 0.05/Gyr.

REFERENCES

Abraham, R. G. et al. 1996 *ApJ*, 471, 694

Abraham, R. G., Ellis, R. S., Fabian, A. C., Tanvir, N. R. & Glazebrook, K. 1998, *MNRAS*, 303, 641

Andreon, S. & Ettori, S. 1999 *ApJ*, 516, 647

Antonuccio-Delogu, V. & Colafrancesco, S. 1994, *ApJ*, 421, 1

Balogh, M. L., Morris, S. L., Yee, H. K. C., Carlberg, R. G. & Ellingson, E. 1997, *ApJ*, 488, L75

Balogh, M. L., Schade, D., Morris, S. L., Yee, H. K. C., Carlberg, R. G. & Ellingson, E. 1998, *ApJ*, 504, L75

Barbaro, G. & Poggianti, B. M. 1997, *A&A*, 324, 490

Barger, A. J., Aragón-Salamanca, A., Ellis, R. S., Couch, W. J., Smail, I., & Sharples, R. M. 1996, *MNRAS*, 279, 1

Barger, A. J., Aragón-Salamanca, A., Smail, I., Ellis, R. S., Couch, W. J., Dressler, A., Oemler, A., Poggianti, B. M. & Sharples, R. M. 1998, *ApJ*, 501, 522

Balsara, D., Livio, M., & O'Dea, C. P. 1994, *ApJ*, 437, 83

Baugh, C. M., Cole, S. & Frenk, C. S. 1996, *MNRAS*, 283, 1361

Bohlin, R. C., Hill, J. K., Jenkins, E. B., Savage, B. D., Snow, T. P. Jr., Spitzer, L. Jr., & York, D. G. 1983, *ApJS*, 51, 277

Böhm-Vitense, E. 1992, *Introduction to Stellar Astrophysics Vol. 3: Stellar Structure and Evolution*, Cambridge University Press, Cambridge, UK., p. 16.

Bothun, G. D., & Dressler, A. 1986, *ApJ*, 301, 57

Bower, R. G., Kodama, T. & Terlevich, A. 1998, *MNRAS*, 299, 1193

Broadhurst, T. J., Ellis, R. S. & Shanks, T. 1988, *MNRAS*, 235, 827

Bruzual, G. A. & Charlot, S. 1993, *ApJ*, 405, 538

Butcher, H., & Oemler, A. 1978, *ApJ*, 219, 18

Butcher, H., & Oemler, A. 1984, *ApJ*, 285, 426

Byrd, G., & Valtonen, M. 1990, *ApJ*, 350, 89

Caldwell, N., Rose, J. A., Sharples, R. M., Ellis, R. S. & Bower, R. G. 1993, *AJ*, 106, 473

Caldwell, N., Rose, J. A. & Dendy, K. 1998, *AJ*, 117, 140

Carlberg, R. G., Yee, H. K. C. & Ellingson, E. 1997, *ApJ*, 478, 462

Carlberg, R. G., Yee, H. K. C., Ellingson, E., Abraham, R., Gravel, P., Morris, S., & Pritchett, C. J. 1996, *ApJ*, 462, 32

Coleman, G. D., Wu, C. & Weedman, D. W. 1980, *ApJS*, 43, 393

Collins, C., Burke, D., Romer, A., Sharples, R. & Nicol, R. 1997, *ApJ*, 479, L117

Couch, W. J., & Sharples, R. M. 1987, *MNRAS*, 229, 423

Couch, W. J., Ellis, R. S., Sharples, R. M. & Smail, I. 1994, *ApJ*, 430, 121

Couch, W. J., Barger, A. J., Smail, I., Ellis, R. S. & Sharples, R. M. 1998, *ApJ*, 497, 188

Crone, M. M., Evrard, A. E., Richstone, D. O. 1994, *ApJ*, 434, 402

Dressler, A. 1980, *ApJ*, 236, 351

Dressler, A. & Gunn, J. E. 1983, *ApJ*, 270, 7

Dressler, A., Oemler, A. Jr., Butcher, H. R. & Gunn, J. E. 1994, *ApJ*, 430, 107

Dressler, A., Oemler, A. Jr., Couch, W. J., Smail, I., Ellis, R. S., Barger, A., Butcher, H., Poggianti, B. M. & Sharples, R. M. 1997, *ApJ*, 490, 577

Dressler, A., Smail, I., Poggianti, B. M., Butcher, H., Couch, W. J., Ellis, R. S. & Oemler, A. 1999, *astro-ph/9901263*

Dressler, A., Thompson, I. B. & Shectman, S. A. 1985, *ApJ*, 288, 481

Efron, B. 1981, *Biometrika*, 68, 589

Efron, B. & Tibshirani, R. 1986, *Statistical Science*, 1, 54

Ellis, R. S., Smail, I., Dressler, A., Couch, W. J., Oemler, A. Jr., Butcher, H., Sharples, R. M. 1997, *ApJ*, 483, 582

Evrard, A. E. 1991, *MNRAS*, 248, 8p

Fabricant, D. G., McClintock, J. E. & Bautz, M. W. 1991, *ApJ*, 381, 33

Fioc, M. & Rocca-Volmerange, B. 1997, *A&A*, 326, 950

Fisher, D., Fabricant, D., Franx, M. & van Dokkum, P. 1998, *ApJ*, 498, 195

Fujita, Y. 1998, *ApJ*, 509, 587

Fujita, Y., Takizawa, M., Nagashima, M. & Enoki, M. 1999, *astro-ph/9904386*

Gavazzi, G., & Jaffe, W. 1987, *ApJ*, 310, 53

Gioia, I. M. & Luppino, G. A. 1994, *ApJS*, 94, 583

Gisler, G. R. 1978, *MNRAS*, 183, 633

Gott, J. R., & Gunn, J. 1972, *ApJ*, 176, 1

Hamilton, D. 1985, *ApJ*, 297, 371

Hammer, F. et al. 1997, *ApJ*, 481, 49

Hashimoto, Y., Oemler, A. Jr., Lin, H. & Tucker, D. L. 1998, *ApJ*, 499, 589

Henriksen, M. J. & Byrd, G. 1996, *ApJ*, 459, 82

Henriksen, M. J. & Jones, C. 1996, *ApJ*, 465, 666

Henry, J. P., Gioia, I., Maccacaro, T. et al. 1992, *ApJ*, 386, 408

Humason, A. J. 1956, *AJ*, 61, 97.

Kauffmann, G. 1995, *MNRAS*, 274, 153

Kelson, D. D., van Dokkum, P. G., Franx, M., Illingworth, G. D. & Fabricant, D. 1997, *ApJ*, 478, L13

Kennicutt, R. C., Jr. 1992a, *ApJ*, 388, 310

Kennicutt, R. C., Jr. 1992b, *ApJS*, 79, 255

Kinney, A. L., Calzetti, D., Bohlin, R. C., McQuade, K., Storchi-Bergmann, T. & Schmitt, H. R. 1996, *ApJ*, 467, 38

King, C. & Ellis, R. S. 1985, *ApJ*, 288, 456

Kodama, T., Bower, R. G. & Bell, E. F. 1998, *MNRAS*, 302, 152

Larson, R. B., Tinsley, B. M. & Caldwell, C. N. 1980, *ApJ*, 237, 692

Lavery, R. J. & Henry, J. P. 1986, *ApJ*, 304, L5

Lewis, A. D., Ellingson, E., Morris, S. L. & Carlberg, R. G. 1999, *ApJ*, 517, 587

Lilly, S. J., Tresse, L., Hammer, F., Crampton, D. & LeFevre, O. 1995, *ApJ*, 455, 108

Lilly, S. J. et al. 1998, *ApJ*, 500, 75

Lin, H., Yee, H. K. C., Carlberg, R. G. & Ellingson, E. 1997, *ApJ*, 475, 494

Lin, H., Yee, H. K. C., Carlberg, R. G., Morris, S. L., Sawicki, M., Patton, D. R., Wirth, G., & Shepherd, C. W. 1999 *ApJ*, 518, 533

MacLaren, I., Ellis, R. S. & Couch, W. J. 1988, *MNRAS*, 230, 249

Moore, B., Katz, N., Lake, G., Dressler, A. & Oemler, A. 1996, *Nature*, 379, 613

Moore, B., Lake, G. & Katz, N. 1998, *ApJ*, 495, 139

Morris, S. L., Hutchings, J. B., Carlberg, R. G., Yee, H. K. C., Ellingson, E., Balogh, M. L., Abraham, R. G. & Smecker-Hane, T. A. 1998, *ApJ*, 507, 84

Moss, C., & Whittle, M. 1993, *ApJ*, 407, L17

Newberry, M. V., Boroson, T. A. & Kirshner, R. P. 1990, *ApJ*, 350, 585

Nulsen, P. E. J. 1982, *MNRAS*, 198, 1007

Osterbrock, D. E. 1960, *ApJ*, 132, 325

Poggianti, B. M. & Barbaro, G. 1996, *A&A*, 317, 379

Poggianti, B. M., Smail, I., Dressler, A., Couch, W. J., Barger, A. J., Butcher, H., Ellis, R. S. & Oemler, A. 1999 *ApJ*, 518, 576

Rakos, K. D. & Schombert, J. M. 1995, *ApJ*, 439, 47

Rieke, G. H., Loken, K., Rieke, M. J. & Tamblyn, P. 1993, *ApJ*, 412, 99

Rosati, P., Della Ceca, R., Norman, C. & Giacconi, R. 1998, *ApJ*, 492, L21

Rowan-Robinson, M. et al. 1997, *MNRAS*, 289, 490

Salpeter, E. E. 1955, *ApJ*, 121, 161

Sharples, R. M., Ellis, R. S., Couch, W. J. & Gray, P. M. 1985, *MNRAS*, 212, 687

Smail, I., Dressler, A., Couch, W. J., Ellis, R. S., Oemler, A., Butcher, H. & Sharples, R. M. 1997, *ApJS*, 110, 213

Smail, I., Edge, A. C., Ellis, R. S. & Blandford, R. D. 1998, *MNRAS*, 293, 124

Torman, G. 1998, *MNRAS*, 297, 648

Tresse, L. & Maddox, S. J. 1998, *ApJ*, 495, 691

Valluri, M. 1993, *ApJ*, 408, 57

Van Haarlem, M. & van de Weygaert, R. 1993, *ApJ*, 418, 544

Vikhlinin, A., McNamara, B., Forman, W., Jones, C., & Quintana, H. 1998, *ApJ*, 498, L21

Whitmore, B. C., Gilmore, D. M., & Jones, C. 1993, *ApJ*, 407, 489

Yee, H. K. C., Ellingson, E., & Carlberg, R. G. 1996, *ApJS*, 102, 269

Yee, H. K. C., Sawicki, M. J., Ellingson, E. & Carlberg, R. G. 1995, *ASP Conference Series*, 86, 301; San Francisco: ASP; A. Buzzoni, A. Renzini & A. Serrano, eds.

Zabludoff, A. I. & Franx, M. 1993, *AJ*, 106, 4

Zabludoff, A. I., Zaritsky, D., Lin, H., Tucker, D., Hashimoto, Y., Shectman, S. A., Oemler, A. & Kirshner, R. P. 1996, *ApJ*, 466, 104